



HAL
open science

Heterogeneous hydraulic conductivity and porosity fields reconstruction through steady-state flow and transient solute transport data using the continuous adjoint state

Frederick Delay, Hamid Badri, Philippe Ackerer

► To cite this version:

Frederick Delay, Hamid Badri, Philippe Ackerer. Heterogeneous hydraulic conductivity and porosity fields reconstruction through steady-state flow and transient solute transport data using the continuous adjoint state. *Advances in Water Resources*, 2019, 127, pp.148-166. 10.1016/j.advwatres.2019.03.014 . hal-03017891

HAL Id: hal-03017891

<https://hal.science/hal-03017891>

Submitted on 22 Oct 2021

HAL is a multi-disciplinary open access archive for the deposit and dissemination of scientific research documents, whether they are published or not. The documents may come from teaching and research institutions in France or abroad, or from public or private research centers.

L'archive ouverte pluridisciplinaire **HAL**, est destinée au dépôt et à la diffusion de documents scientifiques de niveau recherche, publiés ou non, émanant des établissements d'enseignement et de recherche français ou étrangers, des laboratoires publics ou privés.



Distributed under a Creative Commons Attribution - NonCommercial 4.0 International License

1 **Heterogeneous hydraulic conductivity and porosity fields reconstruction through**
2 **steady-state flow and transient solute transport data using the continuous adjoint state**

3 Frederick Delay¹, Hamid Badri, Philippe Ackerer

4 Laboratoire d'Hydrologie et de Géochimie de Strasbourg, Univ. Strasbourg - CNRS.

5 UMR 7517, 1 Rue Blessig, Strasbourg 67000, France

6 ¹ Corresponding author: Phone +33 3 68 85 04 16; Fax +33 3 68 85 04 02; E-mail address: fdelay@unistra.fr

7

8 **Abstract**

9 A parameter estimation methodology has been developed on the basis of model
10 inversion using a Quasi-Newton method and adaptive parameterization. The continuous adjoint
11 state equations for both flow and transport in porous media are employed as the tool calculating
12 the gradient components of the objective function with respect to parameters. **Solving the**
13 **continuous form of the adjoint equations can be implemented independently of the code used**
14 **to solve the forward problem, which renders the technique non-intrusive.**

15 The developed methodology is applied to the identification of hydraulic conductivity
16 and porosity fields conditioned by piezometric head data associated with steady-state flow and
17 transient solute concentrations. Synthetic numerical experiments have been undertaken for test
18 cases of increasing complexity, from an almost uniform flow sweeping the modeled domain
19 with a prescribed uniform continuous injection of solute at the inflow boundary, to spatially
20 highly variable flow conditions obtained through source/sink terms within the flow domain and
21 a local stepwise solute injection. The results of inversions are analyzed using criteria based on
22 the comparisons between estimated concentration and reference concentration values as well as
23 comparisons between estimated hydraulic conductivity (and porosity for one test case) and
24 reference hydraulic conductivity fields.

25 The results show that employing a continuous adjoint state technique computed
26 independently of the direct problem is an efficient option for parameter estimation relying
27 jointly upon flow and transport data. **In the reported numerical examples that are characterized**
28 **by the identifiability of the flow problem on the basis of hydraulic head observations,**
29 **concentration data from solute transport scenarios bring few added value to sought solutions of**
30 **hydraulic conductivities.** The spatial structure of the conductivity fields is slightly improved
31 compared with **the** reference, but the overall system in terms of head distribution, identification
32 of main flow paths, and solute transit times, only inherits cosmetics.

33

34 **Keywords**

35 Parameter estimation, adjoint state, adaptive parametrisation, groundwater, hydraulic
36 conductivity, porosity.

37

38 **Highlights** (less than 85 characters including spaces)

- 39 - The continuous adjoint state associated with the transport equation is derived.
- 40 - Hydraulic conductivity and porosity fields are estimated by inverse modeling.
- 41 - Concentration data complementing heads slightly improve inverse solutions to flow.

42 **1. Introduction**

43 Parameter estimation through inverse methods for flow and solute transport simulations
44 is still challenging despite the variety of concepts and methods developed since the pioneer
45 works in inverse methods of Vemuri et al. (1969), Emsellem and de Marsily (1971), and Yeh
46 and Tauxe (1971), among others. Recent reviews of conceptual frameworks and methods can
47 be found in Hendricks Franssen et al. (2009), Zhou et al. (2014), and Linde et al. (2015). Almost
48 all the developed methods target the estimation of hydraulic conductivities (or transmissivities)
49 constrained (conditioned) by hydraulic heads and, through the last 40 years, by additional data
50 such as solute concentrations, geological information or geophysical properties.

51 In this work, we focus, **as a first goal**, on estimating **spatially-heterogeneous** hydraulic
52 conductivity and porosity fields conditioned by both hydraulic heads and solute concentrations.
53 Many authors have already addressed this challenge, and Table 1 presents an overview of
54 various approaches dedicated to this topic. The table is not an exhaustive presentation of the
55 existing literature but a selection of works (17 contributions ranked as they appear in time in
56 the literature) that we consider representative of methods and trends.

57 **Solving the inverse problem for flow and transport in ground water systems is tightly**
58 **associated with methodological choices.** Among the possible choices, we exemplify, via
59 continuous adjoint state calculations, how gradient-based inversion techniques can cope with
60 highly parameterized problems. Mixing data of various types and weighting them in the
61 objective function of an inverse problem is also a key feature. This is why this study **emphasizes**
62 **methodology as a second goal.**

63 Notably, when modeling natural systems (or synthetic test cases supposedly close to
64 natural systems), it is always complicated to discuss on identifiability, uniqueness of inverse
65 solutions, quality of conditioning, etc., simply because highly parameterized inverse problems
66 encompassing multiple elementary processes result in fuzzy theoretical frameworks. That being

67 said, it cannot be overlooked that complex systems might result in multiple inverse solutions.
68 Repeatability, in the sense of estimating how similar various solutions are when initiated at
69 different locations in the parameter space, appears as a simple way to determine success or
70 failure of inversions. Incidentally, when dealing with synthetic test cases employing fully-
71 known reference problems, the comparison between inverse solutions and references is also
72 informative.

73 In this study, observations associated with flow and transport parameter estimations are
74 scarce piezometric head data from steady-state flow conditions and solute concentrations under
75 transient transport conditions. These data are used to build an objective function assembling
76 two terms: the sum of the weighted squared differences between measured and computed
77 piezometric heads F_h , and the sum of the weighted squared differences between measured and
78 computed solute concentrations F_c . Notably, the weights may sometimes serve to narrow down
79 the range spanned by the squared differences when data of different units are used. This type
80 of objective function is usually employed within: (i) the non-linear Least Square framework,
81 which also often adds a regularization term on model parameters, or (ii) the Maximum
82 Likelihood framework earlier proposed by Carrera and Neuman (1986), which allows for
83 handling prior information on model parameters. Summing two quantities that have different
84 units in an objective function requires an adapted strategy and/or the use of a weighting
85 coefficient applied to one of these terms (usually F_c). In fact, the weighting should be directly
86 given by the probability density functions of errors between model outputs and observations.
87 The point is that these densities are generally conjectured, which results in weights given to F_h
88 and F_c becoming parameters of the inversion procedure. Pioneer works from Umari et al.
89 (1979), Strecker and Chu (1986), and Keidser and Rosbjerg (1991) proposed a two-stage
90 procedure to minimize successively F_h and F_c . Simultaneous inversion of both heads and

91 solute concentrations (and simultaneously decreasing both F_h and F_c) is nowadays the
92 common way to estimate the parameters. Nevertheless, the optimal weighting of the two terms
93 F_h and F_c has been under debate (Carrera and Neuman, 1986; Doherty, 2003; Medina and
94 Carrera, 2003), and is still not fully resolved.

95 Even though abundant literature and many studies are available for other inversion
96 techniques, gradient-based methods are the most common algorithms applied to minimize the
97 objective function. The minimization employs either sensitivity coefficients with a Gauss-
98 Newton method (Levenberg, 1944; Marquardt, 1963) or adjoint state variables coupled with a
99 Quasi-Newton method (Byrd et al., 1994). Over the last decade, Kalman filtering (Kalman,
100 1960) and its extensions such as Ensemble Kalman filtering (e.g., Iglesias et al., 2013; Deng et
101 al., 2016) have been applied and improved to efficiently solve the inverse problem. The method
102 has become a valuable alternative approach to gradient-based methods for estimating flow and
103 transport parameters.

104 Parameterization techniques have also shown an interesting evolution over the last 50
105 years. Zonation was the most popular method during the seventies period, probably due to lack
106 of powerful computers that hampered the deployment of stochastic (Monte Carlo) simulations.
107 Stochastic parameterization now seems to be the standard approach for seeking hydraulic
108 conductivity, but recently, Pool et al. (2015) recalled that zonation could be a relevant option
109 to represent geological patterns for large-scale aquifers (i.e., systems of several tens of km
110 extension with flow patterns modeled at the 100-1000 m scale). In most applications, transport
111 parameters (effective porosity and dispersivities) are usually considered as uniform over the
112 modeled domain, and transport heterogeneity is mainly associated with heterogeneous
113 hydraulic conductivity fields and subsequent variations of the mean fluid velocity in the system.

114 In this work, we explore the capacity of the adaptive parametrization technique detailed
115 in Ackerer and Delay (2010) and Hassane and Ackerer (2017) coupled with an independently

116 computed adjoint equation (Delay et al., 2017) to estimate hydraulic conductivity and porosity
117 spatial distributions conditioned by head and concentration measurements.

118 In the following section, the mathematical models describing the flow and transport
119 processes are presented. Section 3 provides a synopsis of the continuous adjoint state method
120 used to minimize the objective function under the constraints resulting from solving the flow
121 and transport equations. The detailed mathematical development of the continuous adjoint state
122 for transport is reported in Appendix A. It is presented in a new, convenient manner (as done
123 for flow in Delay et al., 2017) that allows for the derivation of the gradient of the objective
124 function with respect to all types of factors, including transport parameters, initial and boundary
125 conditions, and source/sink terms of the transport problem. The objective function and the
126 minimization strategies are presented in Section 4. Finally, the numerical experiments are
127 presented and discussed in Section 5; emphasis is put on the comparison between inverse
128 solutions obtained from calculations conditioned by **head data** only and by the joint use of head
129 and concentration data.

130

131 **2. The forward problem**

132 Steady-state flow and transient transport conditions in a 2D confined aquifer are
133 assumed. These conditions are quite common for practical cases where steady-state flow may
134 represent average flow conditions. These conditions also work for shallow unconfined aquifers
135 that show small variations of water levels (which keep the flow equations linear regarding
136 hydraulic heads). We also assume constant aquifer thickness for simplicity, which allows for
137 inverting hydraulic conductivities instead of transmissivities, but without loss of generality.

138 Under these conditions, groundwater flow and solute transport are modeled over the
139 domain Ω and, for transport, over the time interval $]0, T]$ by (e.g., Bear, 1972):

$$\begin{cases}
\nabla \cdot \mathbf{q} = q_w & \text{over } \Omega \\
\mathbf{q} = -K\nabla h & \\
h = h^D & \text{over } \partial_D \Omega_H \\
-K\nabla h \cdot \mathbf{n}_\Gamma = q_N^w & \text{over } \partial_N \Omega_H
\end{cases} \quad (1)$$

$$\begin{cases}
\frac{\partial \omega c}{\partial t} + \nabla \cdot (\omega \mathbf{u} c - \omega \mathbf{D} \nabla c) = q_c \quad ; \quad \mathbf{u} = \mathbf{q} / \omega & \text{over } \Omega \text{ and }]0, T] \\
c = c^0 & \text{over } \Omega \text{ at } t = 0 \\
c = c_D & \text{over } \partial_D \Omega_C \text{ and }]0, T] \\
-\mathbf{D} \nabla c \cdot \mathbf{n}_\Gamma = q_N^c & \text{over } \partial_N \Omega_C \text{ and }]0, T]
\end{cases} \quad (2)$$

142 where h [L] is the hydraulic head; K [LT^{-1}] is the hydraulic conductivity (considered here as
143 a scalar); q_w [T^{-1}] is the flow source/sink term; c [ML^{-3}] is the concentration; ω [-] is the
144 effective porosity; \mathbf{q} [LT^{-1}] is the Darcy flux; \mathbf{u} [LT^{-1}] is the average water velocity; q_c [ML^{-3}]
145 T^{-1}] is the solute source/sink term; and \mathbf{D} [L^2T^{-1}] is the local dispersion tensor defined by:

$$\begin{aligned}
D_{xx} &= \alpha_L \frac{u_x^2}{\|\mathbf{u}\|} + \alpha_T \frac{u_y^2}{\|\mathbf{u}\|} \\
D_{yy} &= \alpha_T \frac{u_x^2}{\|\mathbf{u}\|} + \alpha_L \frac{u_y^2}{\|\mathbf{u}\|} \\
D_{yx} &= D_{xy} = (\alpha_L - \alpha_T) \frac{u_x u_y}{\|\mathbf{u}\|}
\end{aligned} \quad (3)$$

147 where (u_x, u_y) are the local components of the fluid velocity, $\|\mathbf{u}\|$ is the velocity magnitude
148 and (α_L, α_T) are the longitudinal and transverse dispersities [L], respectively. Dirichlet
149 boundary conditions apply to contours $\partial_D \Omega_H$ for flow and $\partial_D \Omega_C$ for transport as Neumann
150 boundary conditions apply to contours $\partial_N \Omega_H$ for flow and $\partial_N \Omega_C$ for transport. \mathbf{n}_Γ represents
151 the outer vector normal to the contours where Neumann boundary conditions are applied.
152 Boundary conditions and source/sink terms are assumed to be known and prescribed at constant
153 values over time. It is noticeable that for the above equations, the porosity should not vary over
154 time, otherwise flow would no longer be steady-state. Boundary conditions for flow and

155 transport have also been written as independent from one another when it might not be the case.
 156 For example, Neumann boundary conditions for flow with fluxes exiting the domain are often
 157 associated with Neumann boundary conditions for concentrations, but for entering water fluxes,
 158 concentrations are often prescribed via Dirichlet-type boundary conditions.

159

160 **3. Parameter identification methodology**

161 *3.1 The objective function*

162 The parameter identification procedure is based on the minimization of the quadratic
 163 differences between measured and computed variables. These differences are gathered in a so-
 164 called objective function defined as:

$$165 \quad F(\mathbf{p}, \mathbf{h}(\mathbf{p}), \mathbf{c}(\mathbf{p})) = F_h(\mathbf{p}, \mathbf{h}(\mathbf{p})) + \kappa F_c(\mathbf{p}, \mathbf{c}(\mathbf{p})) \quad (4)$$

166 with

$$167 \quad \begin{cases} F_h(\mathbf{p}, \mathbf{h}(\mathbf{p})) = (\hat{\mathbf{h}} - \mathbf{h})^T \mathbf{W}_h (\hat{\mathbf{h}} - \mathbf{h}) \\ F_c(\mathbf{p}, \mathbf{c}(\mathbf{p})) = \sum_{j=1}^{N_t} (\hat{\mathbf{c}}^j - \mathbf{c}^j)^T \mathbf{W}_c^j (\hat{\mathbf{c}}^j - \mathbf{c}^j) \end{cases} \quad (5)$$

168 where $()^T$ denotes the transpose operator; \mathbf{h} and \mathbf{c}^j are the vectors of computed heads and
 169 concentrations with a size corresponding to the number of observations; j is the index of
 170 observation times for transport; N_t is the number of times at which concentrations have been
 171 measured; \mathbf{p} is the vector of parameters (here, hydraulic conductivity and porosity) of size
 172 N_p and $\hat{\mathbf{h}}$ and $\hat{\mathbf{c}}^j$ are the vectors of observed values. $\hat{\mathbf{h}} - \mathbf{h}$ and $\hat{\mathbf{c}}^j - \mathbf{c}^j$ are usually named as
 173 "measurement" errors in the jargon of inverse problems, as they simply are the difference
 174 between model outputs and observations in a framework considering that the model is "exact"
 175 (for a given set of parameters) and data are "flawed". In essence, it must be understood that
 176 measurement errors encapsulate actual errors on measures, differences between model outputs
 177 and data, and the consequences of conceptual errors associated with a model or its settings that

178 are always approximations of reality. Assuming that the measurement errors are not correlated
179 in space and invariant over time, the \mathbf{W} matrices are diagonal, and $w_{kk} = \varepsilon_k^{-1}$, where ε_k is the
180 variance of the measurement errors at location k . Finally, \mathbf{K} is a weighting coefficient to ensure
181 a balanced minimization of both $F_h(\mathbf{p}, \mathbf{h}(\mathbf{p}))$ and $F_c(\mathbf{p}, \mathbf{c}(\mathbf{p}))$. In the framework of the
182 Maximum Likelihood and applying the assumptions made on the \mathbf{W} matrices, \mathbf{K} represents
183 the ratio of the measurement error variance of heads to the measurement errors variance of
184 concentrations. These errors are usually unknown. From a practical standpoint, \mathbf{K} should avoid
185 biased optimization by giving too much importance to either F_h or F_c (Medina and Carrera,
186 2003), and should therefore be modified during the minimization procedure.

187 Different minimization techniques of the objective function $F(\mathbf{p}, \mathbf{h}(\mathbf{p}), \mathbf{c}(\mathbf{p}))$ exist.
188 Because the number of estimated parameters might be large, we rely upon the adjoint state
189 method rendering an estimate of the gradient components of the objective function at a cost
190 independent of the type and the number of parameters (see Appendix A). Even though the
191 convergence toward a minimum of the Quasi-Newton methods is usually slower compared with
192 the Gauss-Newton method (Cooley, 1985), for highly parameterized problems, it is wise to rely
193 upon the adjoint method seeking gradient components which are then introduced into a Quasi-
194 Newton algorithm (Chavent 1979; Neuman and Carrera, 1985; Sun 1994; Ackerer et al., 2014;
195 Sun and Sun, 2015; Delay et al., 2017). Variants of the adjoint state exist (e.g., Medina and
196 Carrera, 2003) to calculate model sensitivity to parameters which then feed Gauss-Newton
197 algorithms. The latter option is not employed here as the calculation costs strongly depend on
198 the number of measurement values.

199

200 *3.2 The continuous adjoint state*

201 The adjoint state technique is associated with the class of problems ensuring the
 202 optimization (minimization) of an objective function under constraints (e.g., Bertsekas, 1996).
 203 These constraints can be, for example, the equations that are solved by a model for which we
 204 seek the optimal parameters rendering model outputs close to observations. Recently, Delay et
 205 al. (2017) presented a thorough discussion on the adjoint state to invert the spatially distributed
 206 problem of flow in dual-porosity systems. Their discussion dealt with both the discrete and
 207 continuous forms of the adjoint state and with a comparison of their ability to assist inversions
 208 in providing rapid calculations of the gradients of the objective function. The present work
 209 inherits the method proposed by Delay et al. (2017) and extends it to the inversion of solute
 210 transport treated via an advection dispersion equation. The adjoint state is employed in its
 211 continuous form, which can be differentiated, and then implemented, without prior knowledge
 212 about the structure of the discrete equations in the forward model.

213 Let us take a forward problem as a continuous operator $\mathcal{V}(c, p) = 0$ handling a single
 214 state variable $c(\mathbf{x}, t)$ and a single type of parameter $p(\mathbf{x}, t)$ over the domain Ω and the period
 215 $]0, T]$. References to space \mathbf{x} and time t coordinates are dropped herein when feasible for better
 216 readability. The objective function of the inverse problem is usually discrete because it
 217 compares a finite set of observations of c with equivalent simulated values (see e.g., Eqs. (4)
 218 and (5)). Nevertheless, the objective function is rewritten in a continuous form

219
$$F(c, p) = \int_0^T \int_{\Omega} f(c, p) d\Omega dt, \text{ with } f \text{ an elementary function, usually piecewise (or pointwise)}$$

220 non-null at locations in time and space where observations are available. It must be noted that
 221 the simple integrals over time and space defining F are here employed for ease of notation,
 222 but without loss of generality. When dealing with discrete objective functions as those in Eq.
 223 (5), the formulation of F becomes complicated with four integrals concealed in the continuous

224 form (see, Delay et al., 2017). For example, with point observations of concentrations \hat{c}_a^b
 225 denoting a value at location \mathbf{X}_a and time t_b , a generalized least-square objective function on
 226 concentrations in a continuous form could be written as:

$$227 \int_0^T \int_0^T \int_{\Omega} \int_{\Omega} \sum_m \sum_n \sum_i \sum_j (c(\mathbf{x}, t) - \hat{c}_m^i) W_{m,n}^{i,j} (c(\mathbf{y}, t') - \hat{c}_n^j) \delta(\mathbf{x} - \mathbf{x}_m) \delta(\mathbf{y} - \mathbf{x}_n) \delta(t - t_i) \delta(t' - t_j) d\mathbf{x} d\mathbf{y} dt dt' \quad (6)$$

228 where $W_{m,n}^{i,j}$ denotes the weight associated with the pair of observations $(\hat{c}_m^i, \hat{c}_n^j)$ and $\delta(\cdot)$ is the
 229 delta-Dirac function.

230 Minimizing the objective function F knowing that the constraint $\mathcal{V}(c, p) = 0$ is
 231 fulfilled, assumes that both the objective function and the constraints are gathered in a
 232 Lagrangian operator in the form:

$$233 \mathcal{L}(c, p, \mu) = \int_0^T \int_{\Omega} f(c, p) d\Omega dt + \int_0^T \int_{\Omega} \mathcal{V}(c, p) \mu d\Omega dt \quad (7)$$

234 As the second term in Eq. (7) is null, the Lagrangian \mathcal{L} is equivalent to the objective function
 235 F , even though it encloses the addition of the constraint \mathcal{V} multiplied by the variable $\mu(\mathbf{x}, t)$
 236 over Ω and $]0, T]$. The variable μ is a Lagrangian multiplier which is defined up to the
 237 addition of a constant or the multiplication by a constant (μ multiplies a constraint expressed
 238 as a null term). The Lagrangian multiplier is named as the continuous adjoint state of the
 239 variable c . If model parameters p are perturbed by δp , with the consequence of generating a
 240 perturbation δc on the variable c , such that $\mathcal{V}(c + \delta c, p + \delta p) = 0$, a variation of the
 241 Lagrangian \mathcal{L} can be written as:

$$242 \delta \mathcal{L} = \int_0^T \int_{\Omega} \frac{\partial f}{\partial c} \delta c d\Omega dt + \int_0^T \int_{\Omega} \frac{\partial f}{\partial p} \delta p d\Omega dt + \int_0^T \int_{\Omega} (\mathcal{V}(c + \delta c, p + \delta p) - \mathcal{V}(c, p)) \mu d\Omega dt \quad (8)$$

243 where a first-order Taylor series expansion has been used to rearrange the terms in f .

244 Identifying the equations ruling the adjoint state μ relies upon the development of the
 245 variations in the constraint $\mathcal{V}(c + \delta c, p + \delta p) - \mathcal{V}(c, p)$ while separating terms in δc from
 246 terms in δp . Cancelling out the terms in δc within $\delta \mathcal{L}$ poses the equations of the continuous
 247 adjoint state over Ω and $[0, T]$ and its initial and boundary conditions. Solving these equations
 248 eliminates terms in δc , which in turn modifies the variation of the Lagrangian that becomes:

$$249 \quad \delta \mathcal{L} = \int_0^T \int_{\Omega} \frac{\partial f}{\partial p} \delta p \, d\Omega dt + \int_0^T \int_{\Omega} \mathcal{G}(c, \mu) \delta p \, d\Omega dt \quad (9)$$

250 with \mathcal{G} a continuous operator combining the state variable c and the adjoint state μ , both
 251 previously calculated by the forward problem and the adjoint state equations, respectively. This
 252 operator \mathcal{G} depends on the type of parameter (the perturbation δp) to which it is associated in
 253 the scalar product in Eq. (8). Usually, parameters in spatially distributed models are defined as
 254 uniform values over subdomains Ω_i of Ω (e.g., zones, cells, etc.) and eventually over periods
 255 Δt_n within $]0, T]$. Denoting p_i^n as the restriction of the parameter $p(\mathbf{x}, t)$ to the subdomain
 256 Ω_i and the period Δt_n , the variation of the Lagrangian $\delta \mathcal{L}$ in Eq. (8) renders an approximation
 257 of the gradient of the objective function with respect to p_i^n

$$258 \quad \frac{\delta \mathcal{L}}{\delta p_i^n} \approx \frac{dF}{dp_i^n} = \int_{\Delta t_n} \int_{\Omega_i} \frac{\partial f}{\partial p_i^n} d\Omega dt + \int_{\Delta t_n} \int_{\Omega_i} \mathcal{G}(c, \mu) d\Omega dt \quad (10)$$

259 where integrals in Eq. (10) are restricted to the subdomain Ω_i and the period Δt_n . It is worth
 260 noting that the adjoint state μ is independent of the type of gradient component dF/dp_i^n to
 261 be calculated. Stated differently and knowing that μ has been calculated beforehand in a single
 262 step very similar to that of the forward model (see below), the access to gradient components
 263 is very rapid, irrespective of the type and the number of sought parameters. This renders the
 264 adjoint state technique suited to highly parameterized problems, when methods based on model

265 sensitivities (the calculation of each sensitivity being very similar to the forward problem) are
 266 plagued by computation costs.

267

268 *3.3 Adjoint state equations and gradients of the objective function*

269 A crucial point of the continuous adjoint state application is in developing the equations
 270 ruling the adjoint state and setting the operators \mathcal{G} mentioned above for calculating the gradient
 271 components. Several attempts have appeared in the literature even though the technique has not
 272 been widely employed in Hydrology. The most important contribution is probably that
 273 proposed by Sun and co-workers (Sun, 1994), who developed the continuous adjoint states for
 274 single-phase flow, two-phase flow, transport under various conditions, and specific applications
 275 targeting the identification of a single type of parameter, a specific form of the objective
 276 function, or steady-state problems. Delay et al. (2017) proposed a unified development (and
 277 presentation) of the continuous adjoint state for flow in dual porosity systems, which became
 278 available for the identification of all types of parameters, initial and boundary conditions, and
 279 source/sink terms. The continuous adjoint state equations for steady-state single-phase flow in
 280 Eq. (1) are an adaptation from Delay et al. (2017). The interested reader is referred to that work
 281 for further details. Regarding the transient solute transport in Eq. (2), the unified development
 282 of the adjoint state equations do not yet appear in the literature and is reported in Appendix A.

283 Regarding the inversion of the coupled problem of steady-state flow and transient
 284 transport, a variation of the continuous Lagrangian operator can be written as:

$$\begin{aligned}
 \delta\mathcal{L}(h, c, \mathbf{p}, \lambda, \mu) = & \int_{\Omega} \frac{\partial f_h}{\partial h} \delta h d\Omega + \int_{\Omega} \frac{\partial f_h}{\partial \mathbf{p}} \delta \mathbf{p} d\Omega + \int_{\Omega} (\mathcal{U}(h + \delta h, \mathbf{p} + \delta \mathbf{p}) - \mathcal{U}(h, \mathbf{p})) \lambda d\Omega \\
 & + \int_0^T \int_{\Omega} \frac{\partial f_c}{\partial c} \delta c d\Omega dt + \int_0^T \int_{\Omega} \frac{\partial f_c}{\partial \mathbf{p}} \delta \mathbf{p} d\Omega dt + \int_0^T \int_{\Omega} (\mathcal{V}(c + \delta c, \mathbf{p} + \delta \mathbf{p}) - \mathcal{V}(c, \mathbf{p})) \mu d\Omega dt
 \end{aligned}
 \tag{11}$$

286 The elementary continuous objective function f has been dissociated in the two components

287 f_h and f_c enclosing the state variable h (head) for flow and the state variable C (concentration)

288 for transport, respectively; $\mathcal{U}(h, p) = 0$ is the continuous steady-state flow equation;
 289 $\mathcal{V}(c, p) = 0$ is the continuous transient-transport equation; λ and μ are the continuous
 290 adjoint states associated with flow and transport, respectively; and \mathbf{p} is the undifferentiated
 291 vector of factors ruling the flow and transport equations. It could include initial and boundary
 292 conditions, source/sink terms, and flow and transport parameters. Here, the aim is to retrieve
 293 hydraulic conductivity (and porosity) fields on the basis of head and concentration
 294 measurements for pre-identified dispersivity parameters, known source/sink terms, and known
 295 initial and boundary conditions. That being said, the hydraulic conductivity influences transport
 296 parameters, such as the mean water velocity \mathbf{u} and the dispersion tensor \mathbf{D} (see Eq. (2)). It
 297 makes sense to calculate via the adjoint state the gradient components of the objective function
 298 with respect to \mathbf{u} and \mathbf{D} and link them with the total variation of the objective function with
 299 respect to K .

300 The continuous adjoint state equations for steady-state flow ruled by Eq. (1) are derived
 301 as (see Delay et al., 2017):

$$302 \quad \begin{cases} \nabla \cdot (-K \nabla \lambda) + \frac{\partial f_h}{\partial h} = 0 & \text{over } \Omega \\ \lambda = 0 & \text{over } \partial_D \Omega_H \\ K \nabla \lambda \cdot \mathbf{n}_\Gamma = 0 & \text{over } \partial_N \Omega_H \end{cases} \quad (12)$$

303 Transport equations in Eq. (2) are flanked with continuous adjoint state equations in the form
 304 (see Appendix A):

$$305 \quad \begin{cases} -\omega \frac{\partial \mu}{\partial t} - \omega \mathbf{u} \cdot \nabla \mu - \nabla \cdot (\omega \mathbf{D} \cdot \nabla \mu) + \frac{\partial f_c}{\partial c} = 0 & \text{over } \Omega \text{ and }]T, 0] \\ \mu = 0 & \text{over } \Omega \text{ at } t = T \\ \mu = 0 & \text{over } \partial_D \Omega_C \text{ and }]T, 0] \\ \mathbf{D} \cdot \nabla \mu \cdot \mathbf{n}_\Gamma = 0 & \text{over } \partial_N \Omega_C \text{ and }]T, 0] \end{cases} \quad (13)$$

306 The minus signs appearing in Eq. (13) for terms in $\partial/\partial t$ and in $\mathbf{u}\cdot\nabla$ assume that Eq. (13) is
307 solved backward over time from T to 0 and with a reversed water velocity field $-\mathbf{u}$. Otherwise,
308 Eq. (13) lacks physical meaning by letting a negative diffusion tensor appear.

309 As told earlier, continuous adjoint state equations look very similar to their equivalent
310 forward problem in Eqs. (1) and (2). Eqs (12) and (13) can be solved numerically by any means
311 (any discretization and numerical scheme) independent of the way the forward problem is
312 solved. The forward model and the adjoint state calculations can be decoupled, which is not the
313 case of the discrete adjoint state technique which is differentiated (from) and calculated with
314 the same discrete equations as those of the forward model (e.g., Ackerer et al., 2014). For its
315 part, the independent implementation of the continuous adjoint state is able to work with any
316 forward model. Both simply exchange information, such as the source/sink terms of the adjoint
317 states, $\partial f_h/\partial h$ and $\partial f_c/\partial c$, those inheriting from calculations performed by the forward model.
318 Notably, Eqs. (12) and (13) show that initial and boundary conditions for the adjoint states are
319 always null. Stated differently, we can say that adjoint states let local source/sink terms diffuse
320 or transport over domains that are partly disconnected from the domain of the forward problem.
321 One might, for example, invert part of the forward problem on a restriction of its domain of
322 definition by simply calculating the continuous adjoint states on this restriction with appropriate
323 types of boundary conditions.

324 With steady-state flow and transient transport aimed at retrieving hydraulic conductivity
325 fields with known porosity and dispersivity transport parameters as well as known initial and
326 boundary conditions, the gradient components of the objective function are of two types:
327 dF_h/dK linking heads with hydraulic conductivity, and dF_c/dK linking concentrations with
328 hydraulic conductivity via the mean water velocity \mathbf{u} and the dispersion tensor \mathbf{D} . For the

329 part of the objective function handling measured and simulated heads, the gradient component
 330 with respect to K is given by (see Delay et al., 2017):

$$331 \quad \frac{dF_h}{dK} = \int_{\Omega} \frac{\partial f}{\partial K} d\Omega + \int_{\Omega} \nabla h \cdot \nabla \lambda d\Omega \quad (14)$$

332 If there is no information (or no prior guess) on hydraulic conductivity values and their
 333 comparison with sought values, the term $\partial f / \partial K$ cancels out in Eq. (14) and the gradient
 334 component of the objective function is a simple scalar product between simulated heads and
 335 the associated adjoint state. For the part of the objective function handling concentrations, the
 336 gradient component with respect to K can be obtained as:

$$337 \quad \frac{dF_c}{dK} = \frac{\partial F_c}{\partial K} \Big|_u + \frac{\partial F_c}{\partial K} \Big|_{\mathbf{D}} \quad (15)$$

338 with

$$339 \quad \frac{\partial F_c}{\partial \mathbf{u}} = - \int_0^T \int_{\Omega} \omega c \nabla \mu d\Omega dt \Rightarrow \frac{\partial F_c}{\partial K} \Big|_u = \left(\frac{\partial F_c}{\partial \mathbf{u}} \right)^T \cdot \frac{\partial \mathbf{u}}{\partial K} = \int_0^T \int_{\Omega} c (\nabla \mu)^T \cdot \nabla h d\Omega dt \quad (16)$$

$$340 \quad \frac{\partial F_c}{\partial \mathbf{D}} = \int_0^T \int_{\Omega} \omega \nabla c \cdot (\nabla \mu)^T d\Omega dt \Rightarrow \frac{\partial F_c}{\partial K} \Big|_{\mathbf{D}} = \int_0^T \int_{\Omega} \omega (\nabla \mu)^T \cdot \frac{\partial \mathbf{D}}{\partial K} \cdot \nabla c d\Omega dt \quad (17)$$

$$\frac{\partial \mathbf{D}}{\partial K} = \frac{\partial \mathbf{D}}{\partial u_x} \frac{\partial u_x}{\partial K} + \frac{\partial \mathbf{D}}{\partial u_y} \frac{\partial u_y}{\partial K} = -\omega^{-1} \frac{\partial \mathbf{D}}{\partial u_x} \frac{\partial h}{\partial x} - \omega^{-1} \frac{\partial \mathbf{D}}{\partial u_y} \frac{\partial h}{\partial y}$$

341 and

$$342 \quad \begin{aligned} \frac{\partial D_{xx}}{\partial u_x} &= \frac{u_x}{\|\mathbf{u}\|^3} (\alpha_L (u_x^2 + 2u_y^2) - \alpha_T u_y^2) & \frac{\partial D_{yy}}{\partial u_x} &= \frac{u_x}{\|\mathbf{u}\|^3} (\alpha_T (u_x^2 + 2u_y^2) - \alpha_L u_y^2) \\ \frac{\partial D_{xy}}{\partial u_x} &= \frac{\partial D_{yx}}{\partial u_x} = (\alpha_L - \alpha_T) \frac{u_y^3}{\|\mathbf{u}\|^3} & & \\ \frac{\partial D_{xx}}{\partial u_y} &= \frac{u_y}{\|\mathbf{u}\|^3} (\alpha_T (u_y^2 + 2u_x^2) - \alpha_L u_x^2) & \frac{\partial D_{yy}}{\partial u_y} &= \frac{u_y}{\|\mathbf{u}\|^3} (\alpha_L (u_y^2 + 2u_x^2) - \alpha_T u_x^2) \\ \frac{\partial D_{xy}}{\partial u_y} &= \frac{\partial D_{yx}}{\partial u_y} = (\alpha_L - \alpha_T) \frac{u_x^3}{\|\mathbf{u}\|^3} & & \end{aligned} \quad (18)$$

343 The gradient components of the objective function with respect to transport parameters,
344 source/sink terms, and initial and boundary conditions are derived in Appendix A. As
345 mentioned earlier, the non-intrusive character of the continuous adjoint state implies exchanges
346 of information between the forward model and the adjoint state. This is also exemplified by the
347 relations of Eq. (14) to Eq. (17), showing that gradient components of the objective function
348 combine values of the state variables calculated by the forward model and values of the adjoint
349 states.

350

351 **4. Parameter estimation strategy**

352

353 The objective function defined by Eq. (4) is a sum of two terms, depending on two very
354 different quantities: piezometric heads expressed as a length and concentrations expressed as
355 mass or moles per volume. In addition to differences in measurement units, the numerical values
356 can also be significantly different. As an example, a difference of 1.0 m between computed and
357 measured heads for heads varying between 100 m and 110 m is less significant than a difference
358 of 1.0 mg.l⁻¹ between computed and measured concentrations for values varying between 0.0
359 mg.l⁻¹ and 2.0 mg.l⁻¹.

360 In the context of the Maximum Likelihood or Generalized Least Squares with
361 regularization, the coefficient κ in Eq. (4) has a physical meaning if the priors on measurement
362 errors are known. However, this information is not often available. Doherty (2003) and Carrera
363 and Neuman (1986) suggested including this coefficient in the parameter estimation procedure.
364 Medina and Carrera (2003) analyzed the optimal weight for identifying hydraulic conductivities
365 conditioned by piezometric heads and concentrations, and they tested different values. The
366 expected value of the likelihood function provides robust weights to be assigned to

367 concentration and hydraulic conductivity data, except for the steady-state flow case. We
368 followed the suggestion of Medina and Carrera (2003) and define the weighting coefficient as:

$$369 \quad \kappa^{k+1} = \frac{\theta}{F_h^k(\mathbf{p}, \mathbf{h}(\mathbf{p})) + F_c^k(\mathbf{p}, \mathbf{c}(\mathbf{p}))} \quad (19)$$

370 where θ is a user-defined variable, and k is the iteration index in the optimization procedure.

371 An alternative to evaluating hydraulic parameters using both types of data h and c is to
372 consider $F_h(\mathbf{p}, \mathbf{h}(\mathbf{p}))$ and $F_c(\mathbf{p}, \mathbf{c}(\mathbf{p}))$ separately. The algorithm suggested by Strecker and Chu
373 (1986), for example, consists of a first stage, which estimates hydraulic conductivities
374 conditioned by heads only, and then is followed by a second stage, which estimates hydraulic
375 conductivities conditioned by concentrations only. In this work, we investigate the performance
376 of the following strategies:

- 377 - **S1**: hydraulic conductivities are estimated using head data only.
- 378 - **S2**: hydraulic conductivities are estimated using head and concentration data
379 simultaneously.
- 380 - **S3**: the conditioning is alternated during the minimization in the sense that a first
381 set of M_h iterations considers head data only, which is then followed by M_c
382 iterations handling both head and concentration data; this swap is repeated until
383 convergence. In this work, we set $M_h=20$ and $M_c=5$. Alternated conditioning
384 suggests that a highly flawed flow field could result in simulated concentrations
385 far from data and eventual problems of convergence. Thus, iterations handling
386 head data only should **first rough-out** the flow field, then refined **by** using both
387 heads and concentrations. The number of iterations for each type of conditioning
388 is problem dependent. This number was chosen by trials counting solutions that
389 converge for 10 runs started at different locations in the parameter space, and
390 also counting the mean number of iterations required per solution to converge.

391 Notably, we did not **delineate** any strategy seeking hydraulic conductivity on the basis
392 **of** concentration measurements only. In general, when concentrations are measured in open
393 wells over a groundwater system, measures of heads in those wells are also available. It would
394 be counter-productive to discard head data. On **the other hand**, there exist many actual systems
395 where concentrations are never monitored. Another reason is that **seeking** hydraulic
396 conductivity fields only via concentration measurements is **usually** not a convergence problem.
397 Concentration distributions over time and space depend on the velocity field, a quantity defined
398 as the product of conductivity and head gradient. Lack of information on heads can result in
399 many hydraulic conductivity fields rendering the same model outputs. **In other words**,
400 concentrations mainly inform on transit times between two locations along a flow line. This
401 time is insensitive to various distributions of the velocities along the line, provided their
402 harmonic means are similar. Therefore, with smoothly varying head gradients, many
403 distribution of hydraulic conductivities along a flow line would result in the same transit times.
404 That being said, heads along a flow line are also mainly controlled by the harmonic mean of
405 conductivities. The point is that the flow equation is diffusive. Widespread head data inform on
406 mean conductivities along all the segments joining the pairs of observations with a consequence
407 of a better deciphering of hydraulic conductivity distributions.

408

409 **5. Numerical experiments**

410 We rely upon synthetic test cases to evaluate the performance of the parameter
411 estimation methodology. Measurement errors in data (as they could be defined here by adding
412 random fluctuations to heads and concentrations extracted from the reference problems) are not
413 considered in the inversion exercises as we mainly focus on comparisons between inversion
414 strategies in their ability to identify reference parameter fields over diverse flow and transport
415 conditions. **In the context of inverse problems, the notion of measurement errors is often taken**

416 as the difference between outputs of a supposedly "exact" model and "flawed" data. Therefore,
417 the absence of noisy measures does not go against the use of an objective function inheriting
418 from the notion of measurement errors.

419

420 *5.1 Settings of the test cases*

421 The synthetic examples investigate a rectangular flow domain of 250 m in length and
422 150 m in width. The aquifer thickness is constant at 20 m. The domain is discretized by a mesh
423 with 1,566 triangular elements of 8 m average length. Four test cases are designed with
424 increasing complexity in the flow field and the solute transport conditions (Table 2).

425 The boundary conditions for flow are a prescribed uniform head of 100 m at the west
426 boundary and a constant over time uniformly distributed outflow rate of $2 \times 10^{-3} \text{ m}^3 \cdot \text{s}^{-1}$ over the
427 east boundary. The north and south boundaries are considered as impervious (see Fig 1). The
428 hydraulic conductivity field follows a log-normal statistical distribution generated with an
429 exponential isotropic covariance function with an effective correlation length of 60 m and a
430 variance of $\sigma_{\log(K)}^2 = 0.12$. Hydraulic conductivity values vary between $3 \times 10^{-3} \text{ ms}^{-1}$ and 10^{-5} ms^{-1}
431 (Fig. 2). Usually, sequential Gaussian simulation techniques, when generating random fields
432 over a rough mesh, do not fully match the prescribed covariance. In practice, the effective
433 covariance (variogram) of the reference hydraulic conductivity field is slightly distorted and
434 shows a correlation length of approximately 85 m, but the right prescribed variance. This feature
435 is unimportant when the question is to retrieve a reference parameter field via inversion without
436 any prior guess on its structure. In the case of inversion exercises seeking both hydraulic
437 conductivity and porosity fields, the reference porosity field follows a normal distribution
438 generated with a spherical covariance function that has a correlation length of 80 m and a
439 variance $\sigma_w^2 = 0.002$. Porosity values vary between 0.04 and 0.36 (Fig. 2), and, as for hydraulic
440 conductivity, the effective covariance is slightly distorted with an effective correlation length

441 of 100 m. Steady-state flow is considered. The test case C1 is designed without source/sink
442 terms whereas five pumping wells and two injection wells (locations in Fig. 1) are added in the
443 domain for the other test cases C2 and C3 (see Table 2). Pumping and injection rates are set to
444 $5.55 \times 10^{-3} \text{ m}^3 \cdot \text{s}^{-1}$. The mathematical model for flow is solved using mixed finite elements
445 (Younes et al., 2010) with a code developed in the lab and checked for being rigorously mass-
446 conservative at the scale of each cell of the mesh.

447 It is worth noting that all the settings employed to generate the various flow fields are
448 **assumed** to render a well-posed problem for the inversion of hydraulic conductivities. The
449 existence of source/sink terms or Neumann boundary conditions in the flow equations avoids
450 the evaluation of conductivity up to the multiplication by a constant. Nevertheless, with only
451 20 head values available for the identification of more than 1500 parameters (in essence, one
452 per cell of the discretized domain, noting those 1500 values are not independent), good
453 inversion results are not guaranteed. This motivates to complement the head data set with
454 concentrations from transport scenarios. Incidentally, rendering the flow field tortuous by
455 adding injection/pumping wells in the system (tests cases C2 and C3) is supposed to complicate
456 the inversion using head data only. In these test cases, concentrations following the main flow
457 paths are expected to increase the degree of improvement of the inverse solutions conditioned
458 on heads only.

459 Regarding the simulation of solute transport, a null dispersive flux is set at all
460 boundaries except at the line $x=0 \text{ m}$, $y \in [25;125]$ where a concentration of $1 \text{ kg} \cdot \text{m}^{-3}$ is
461 prescribed for test cases C1 and C2, and at the upstream (western) flow boundary of test case
462 C3 where the solute concentration is set to zero. For test case C3, a pulse of solute is injected
463 over a rectangular domain of delineation $x \in [5,10] \text{ m}$ and $y \in [65,85] \text{ m}$ during 2 days with a
464 rate of $8.0 \times 10^{-3} \text{ kg} \cdot \text{m}^{-3} \cdot \text{s}^{-1}$. The transport parameters are homogeneous and assumed to be

465 known for test cases C1, C2, and C3. The effective porosity is equal to 0.05 and the longitudinal
466 and transverse dispersivities are $\alpha_L=10$ m and $\alpha_T=1$ m, respectively. Notably, test case C4 re-
467 handles the settings of test case C2, but adds an unknown heterogeneous porosity field to be
468 retrieved in addition to the hydraulic conductivity field. For all test cases, the solute transport
469 simulations are run under transient conditions with initial null concentrations within the system,
470 and the simulations are performed over 120 days. The transport equations are solved using a
471 combination of mixed and discontinuous finite elements methods, which limits the effects of
472 numerical dispersion (Hassane et al., 2017).

473 Steady-state hydraulic heads and time-varying concentrations are observed at 20 wells
474 (see Fig. 1) uniformly distributed in the domain. Concentrations are sampled every day. Overall,
475 the observations consist of 20 head values and $20 \times 120 = 2400$ concentration values. It is worth
476 noting that a large number of data points, as is the case here for concentration values, can
477 mislead the inversion procedure when the corresponding computed variables are not sensitive
478 to the parameter values, as, for example, close to the boundary conditions. The weighting
479 parameter θ in the \mathcal{K} coefficient of the objective function (see Eq. (19)) is set to 10^{-4} for each
480 test case.

481 The initial parameter mesh of the adaptive parameterization (see, e.g., Ackerer and
482 Delay, 2010) consists of 12 triangular elements and 11 nodes uniformly distributed over the
483 domain. The parameter mesh is refined 3 times and the total number of estimated hydraulic
484 conductivities, which may vary between runs according to the way the parameter mesh is
485 refined, is between approximately 60 and 80. Each inversion is repeated 50 times, and the initial
486 parameter grid is assigned with initial parameter values chosen randomly in a uniform
487 distribution. The aim of this duplication is to evaluate the reproducibility of the results and
488 compare them to the reference. The sought hydraulic conductivity values are bounded between
489 1.0×10^{-5} m.s⁻¹ and 3.0×10^{-3} m.s⁻¹ during inversion, and for test case C4, porosity is sought in

490 the range [0.01, 0.40]. These upper and lower bounds of hydraulic conductivities and porosities
491 are the only prior information on parameters brought to the inversion procedure.

492 Adjoint state variables associated with both flow and transport are computed with a
493 different numerical code but with the same grid and the same numerical methods as those
494 employed for the calculation of the state variables. Codes for the adjoint states were developed
495 in the lab as tools independent of the forward codes with the aim of building an inversion
496 toolbox *working in parallel with* any forward model, even on non-proprietary codes for which
497 the calculation structures are unknown. Separate codes between the forward problem and the
498 adjoint state calculations also allowed us to check how the exchanges of information between
499 the grids of adjoint states and that of the forward flow and transport models could eventually
500 hamper inversions (see e.g., Delay et al., 2017). This feature is not reported in this study as both
501 the forward problems and adjoint state calculations share the same computation grids with
502 exchanges of information free from any interpolation.

503

504 *5.2. Inversion of the hydraulic conductivity with known uniform porosity*

505 The settings of the test cases are motivated by three objectives that are: (i) to evaluate
506 the different strategies for estimating the parameters (strategies S1 to S3), (ii) to assess the
507 effects of flow conditions by comparing test cases C1 and C2, and (iii) to assess the effects of
508 transport boundary conditions by comparing test cases C2 to C3.

509 Irrespective of the addressed test cases, the observed hydraulic heads are always
510 *matched within* an error of 5-10 cm for maximal variations of heads over the flow fields of
511 approximately 2 m. This very good matching (see also a comparison of heads between inverted
512 and reference flow fields in Fig. 3) justifies that results on heads will not be addressed in the
513 following discussion. Consequently, the comparisons are based on different criteria and only
514 involve concentration and hydraulic conductivities. These criteria deal with the overall spatial

515 distribution of concentrations at a given time, the analysis of breakthrough curves (BTC) at 3
516 locations (see Fig. 1), and the calibrated parameter fields compared with the reference. Fifty
517 different solutions per test were analyzed. These solutions were obtained by starting the
518 inversion procedure from **different randomly picked locations** in the parameter space. It is also
519 worth noting that the multiscale parameterization randomizes the current inverse solution each
520 time the parameter grid is refined. These solutions cannot be distinguished in view of the final
521 values of the objective function, meaning that they are of similar quality in terms of quadratic
522 differences between the reference and estimated heads and concentrations.

523 Regarding solute concentrations, the BTC stemming from 50 solutions were gathered
524 into a confidence interval computed for each time step n and defined by $[\langle c^n \rangle \pm \sigma_{c^n}]$ where $\langle c^n \rangle$
525 is the mean of the 50 concentration values at time step n , and σ_{c^n} is the corresponding standard
526 deviation. Preliminary computations show that the confidence intervals did not change
527 significantly by running more simulations. With these 50 realizations, an average value of the
528 decimal logarithm of the hydraulic conductivity $\langle \log(\tilde{K}_E) \rangle$ was computed for each element E
529 of the mesh with its associated standard deviation. An average error for each element E $\langle \varepsilon_E \rangle$
530 was also used as an assessment criterion and defined by:

$$531 \quad \langle \varepsilon_E \rangle = \langle \log(\tilde{K}_E) \rangle - \log(K_E) \quad (20)$$

532 where K_E is the exact value (from the reference field) of the hydraulic conductivity at element
533 E , and \tilde{K}_E is the estimated value. The variograms of $\log(\tilde{K}_E)$ were also compared with the
534 reference as an overall indicator of quality of estimated parameter fields. In the same way as
535 for breakthrough curves, the 50 variogram functions were gathered into a confidence interval
536 for each lag.

537 The concentration distributions are provided in Fig. 3. The main features of the
538 reference concentration distributions are reproduced by the inverse solutions for all test cases

539 and all inversion strategies (regarding the objective function). However, the estimated
540 concentrations show additional smearing compared with the reference even though the same
541 mesh and same dispersivities were used for calculating reference and inverse solutions. As
542 shown hereafter, the retrieved hydraulic conductivity fields are smoother than the reference.
543 This feature is consistent with the robustness of the flow equation with respect to hydraulic
544 conductivity, in the sense that the head variable is not very sensitive to local contrasts in
545 hydraulic conductivity values (e.g., Giudici and Vassena, 2008).

546 The strategy overlooking concentration data in the objective function (S1) provides
547 results as good as the other strategies accounting for concentrations in test cases C1 and C3;
548 however, in test case C2, the effects of the injection wells are not completely reproduced. The
549 quality of the match for test case C3 is still quite good, even though solute concentrations remain
550 null for some observation wells that are not downstream of the local injection source. This
551 means that including observations at locations that do not see any concentrations is helpful to
552 retrieve the fluid velocity field and its subsequent relationship with hydraulic conductivities.

553 The different strategies can be distinguished when considering BTC (Figs. 4 to 6) as a
554 quality criterion of the parameter estimation. For test case C1 (Fig. 4), the BTC are well
555 reproduced when employing the two strategies S1 and S2. For strategy S3, which consists of
556 incorporating concentration data in the objective function while calculating the first iterations
557 of convergence by relying upon head data only, the method results in a few discrepancies
558 regarding the arrival times of concentrations. This bias on arrival times also occurs with strategy
559 S1 (concentration data are never used) and test case C2 (Fig. 5). These two attempts show that
560 concentration data provide useful and valuable information on solute travel times, which in turn
561 inform on hydraulic conductivity values.

562 Test case C3 is harder to decipher because solute concentrations remain equal to the
563 initial conditions (null concentration values) at a significant number of monitored wells not

564 located downstream of the local injection. Therefore, test case C3 is more sensitive to flow
565 direction variations within the domain than test cases C1 and C2. A poor estimation of the flow
566 direction in test case C3 leads to either a difference in mean travel time or a difference in the
567 total solute "mass" passing through the wells (the mass being defined as the integral of the BTC
568 over time). Discrepancies in mass can be observed at wells P7 and P9 (except for strategy S2).
569 Again, strategy S2, which includes weighted information on both head and concentration data
570 in the objective function, is the most efficient strategy to retrieve the flow field. It is worth
571 noting that for all test cases and all strategies, the early arrival times of concentrations are well
572 estimated. The accuracy of the estimated parameters decreases with the travel distance (late
573 arrival times) as shown by the increase in the range of the confidence interval from well P11 to
574 well P9 for test cases C1 and C2.

575 The estimated hydraulic conductivities are analyzed by comparing the average value of
576 $\log(K)$, its related standard deviation, and the average error in Eq. (20) (Figs. 7 to 9). The
577 three test cases provide very similar results, showing that:

- 578 - In general, the hydraulic conductivity field is fairly well reproduced irrespective
579 of the inversion strategy employed.
- 580 - The largest differences between estimated and reference $\log(K)$ are located
581 close to the eastern boundary of the domain assigned with a prescribed flux for
582 flow. At these locations, fluxes remain almost similar irrespective of the local
583 conductivity values. The reliability of the estimated parameters, measured by the
584 local standard deviation of $\log(K)$, is poor (high standard deviation) in this
585 eastern area compared with the rest of the domain. It is also worth noting that
586 after 120 days of transport, solute concentrations did not reach the eastern
587 boundary and thus poorly inform the inverse problem on local hydraulic
588 conductivity experienced during transport. This could be an additional

589 explanation for the poor evaluation of conductivities close to the eastern
590 boundary of the domain.

- 591 - The third strategy, S3, leads to the poorest parameter estimation compared with
592 the other two.
- 593 - The ensemble of inverse solutions is wider for strategy S2 than for strategy S1
594 (see test cases C2 and C3 in Figs. 8 and 9). These results may appear counter-
595 intuitive as it is usually expected that more information (of good quality) brought
596 to the inverse problem should yield better results, or at least more constrained
597 solutions (which **is consistent** with the robustness of these solutions). This
598 notwithstanding, the additional information provided by concentrations does not
599 have the same meaning as information on heads. In short, concentrations are
600 sensitive to flow directions and associated travel times along these directions as
601 heads are sensitive to conductivities in a neighborhood roughly centered on the
602 head measurement location. Increasing the complexity of the inverse problem
603 by multiplying the number of sensitive factors or phenomena is conducive to an
604 increase of local minima. This feature spreads out the set of possible inverse
605 solutions even though these solutions resulted in similar values of the objective
606 function.

607 Finally, the results were analyzed via a global criterion, comparing the variogram of
608 $\log(K)$ from the reference solution to the variograms computed from the estimated solutions
609 (Fig. 10). All variograms from inverse solutions underestimate the spatial variability of
610 hydraulic conductivities within lag distances less than one-half the size of the domain. This
611 feature is consistent with the fact evoked above stating that hydraulic head fields are not very
612 sensitive to local contrasts in hydraulic conductivity values. In addition, concentrations at a
613 given time and location depend on the average travel time between the source and the

614 observation well. Therefore, they are rather less sensitive to local hydraulic conductivity
615 variations than to the mean of conductivities experienced along the flow path between injection
616 and observation. This could explain the inference of smaller variances for variograms from
617 inverted conductivity fields. In the same vein, hydraulic heads, as the variables of a diffusion
618 process (Darcian flow), are known to be rather more sensitive to mean values of conductivities
619 over large patches than to contrasts between local values.

620

621 *5.3 Identification of hydraulic conductivity and effective porosity distributions*

622 The additional test case C4 re-handles the settings of test case C2 but considers the
623 inversion of both the hydraulic conductivity field and a heterogeneous effective porosity field.
624 A single strategy S2 was employed to estimate the parameters, with the minimization in a single
625 phase of an objective function mixing both hydraulic head and concentration data (Eq. (4)).
626 This choice of a single strategy is motivated by the inversions of hydraulic conductivity fields
627 that showed strategy S2 to be the most efficient (even though the three strategies employed
628 render almost similar results). It was thought that strategy S2 would also be the best suited to
629 the joint inversion of hydraulic conductivity and porosity. As the mean porosity of the
630 heterogeneous field is approximately 0.12-0.15 in the western half of the domain compared
631 with the uniform value of 0.05 in test case C2, the simulation time for transport is increased up
632 to 280 days (120 days for test case C2) to let the solute plume widely invade the system.

633 The reliability of the simulated concentrations (Figs. 11 and 12) and of the estimated
634 parameters (Figs. 13 and 14) has been significantly diminished compared with the test cases
635 solely inverting hydraulic conductivities. This can tentatively be explained by several features,
636 among which the most likely is that the main driver to solute concentration propagation is the
637 mean water velocity, which depends on the ratio of hydraulic conductivity to effective porosity.
638 It is always challenging to identify both terms of a ratio when the latter is the sensitive

639 parameter, even though both terms of the ratio in the present study are independent quantities
640 with different correlation lengths, etc. It is worth noting that actual data may show relationships
641 between porosity and conductivity values, following for example the well-known Archie's law
642 in its various forms. However, these relationships mainly apply to the fine scale of core samples,
643 but rarely apply to the elementary mesh of a regional aquifer model. In the latter case, small
644 variations in porosity values do not generate enough variability in hydraulic conductivities that
645 might vary over orders of magnitude. That being said, it seems that choosing independent
646 porosity and conductivities values does not help/hamper inversion more than choosing loosely
647 correlated values. Another feature hampering inversion is the increased number of sought
648 parameters, which is approximately 70 hydraulic conductivity values in test case C2 inversions
649 and becomes approximately 210 (in our tests with two independent parameter grids, one for
650 conductivity and one for porosity) in test case C4 inversions.

651 The difficulties experienced by the inverse procedure in test case C4 are also witnessed
652 by the important variability in the estimated concentrations resulting from flow and transport
653 through solution parameter fields (Fig. 12). The spreading of the 50 different possible solutions,
654 and the mean local errors between solutions and the reference are also enlarged (compare, for
655 $\log(K)$ plots, Fig. 13 and test case C2-S2 in Fig. 8). The variograms of the solution parameter
656 fields (Fig. 14) render the same appraisal by underestimating the variability at small scales
657 (small lag-distances). They also highlight the difficulty in estimating with confidence the spatial
658 distribution of porosity.

659

660 **6. Conclusion**

661 We have provided a rigorous and detailed presentation of the partial differential
662 equations ruling the continuous adjoint state associated with solute transport. The adjoint state
663 obeys an advection-dispersion equation that must be solved backward in time and with a

664 reversed flow field compared to the forward problem of transport. It also obeys specific
665 boundary conditions. It can be identified uniquely in a single calculation very similar to that of
666 the forward problem; then, it can serve as calculations for all gradients of the objective function
667 with respect to parameters, initial and boundary conditions, and source/sink terms. We have
668 also extended the adaptive parameterization technique to solute transport and to coupled
669 inversion of flow and transport data. The methodology has been applied to four synthetic test
670 cases targeting the estimation of hydraulic conductivity and effective porosity fields, using both
671 piezometric heads and solute concentration data. These numerical experiments showed:

672 1. Employing the continuous adjoint state solved via an independent numerical code, that is, in
673 a non-intrusive way with regard to existing (proprietary) transport models, is a viable alternative
674 to more common methods (Gauss-Newton and Quasi-Newton methods with embedded
675 computations of sensitivities or adjoint variables) for joint parameter estimation.

676 2. Concentration data has to be taken into account in the parameter estimation and included in
677 the objective function in a balanced way. If the objective function is not weighted, usually
678 hydraulic head observations are rapidly fitted by the inverse procedure, and the conditioning by
679 concentrations will not bring any additional information. In the weighting procedure, the
680 weighting coefficient can be adapted during the minimization and is not necessarily a parameter
681 to include in the minimization.

682 3. Concentration data render information on travel times and flow directions as a valuable
683 means to improve the inference of unknown hydraulic conductivity fields. Null concentrations
684 at some locations are also helpful. In the process of incorporating transport data to retrieve
685 conductivity fields, it could be conjectured that a poor prior knowledge of the fluid velocity
686 field could mislead the inversion relying upon transport data. The consequence would be to
687 partly separate the inversion procedure in a first step, predefining the flow field (conductivities)
688 on the basis of hydraulic head measurements; then, in a second step, launching calculations of

689 transport. Even though successes of inversions are problem dependent, we have shown that the
690 above conjecture is wrong. It is wise to invert both flow and transport scenarios in the same
691 procedure, which means that the objective function of the inverse problem should mix
692 information on heads and concentrations. The objective function would then be minimized in a
693 single phase, handling both terms in heads and concentrations.

694 4. In the test cases reported by this study, it is worth noting that hydraulic head observations
695 were always rapidly fitted, and when used alone, these data rendered valuable hydraulic
696 conductivity fields. The addition of concentration data in the inversion procedure brought few
697 cosmetic features to the conductivity fields, except for better assessment of early and mean
698 travel times in the system, which applies to both sweeping-uniform or tortuous flow fields. A
699 key question raised by this study can be formulated as: Is it worth a try to include concentration
700 data for identifying hydraulic conductivities when it is known how cumbersome and costly
701 concentration measurements can be?

702

703 **Acknowledgments**

704 The authors are indebted to the Qatar National Research Foundation (QNRF) for partly funding
705 this study under the grant NPRP9-030-1-008 "Dual porosity modeling of Qatar karst aquifers".

706 This study is also a contribution to the GEOTREF project funded by the French government in
707 the **framework** of the "Investissements d'Avenir" program and tutored by ADEME.

708

709 **Appendix A**

710 The development of the continuous adjoint state associated with the advection-
 711 dispersion equation for solute transport in porous media is presented below. The continuous
 712 expressions of the gradient components of the objective function are also provided.

713 The continuous operator that solves solute transport and that represents the constraint
 714 $\mathcal{V}(c, \mathbf{p}) = 0$ in the Lagrangian operator of an optimization problem is written as:

$$715 \quad \mathcal{V}(c, \mathbf{p}) = 0 \equiv \frac{\partial \omega c}{\partial t} + \nabla \cdot (\omega \mathbf{u} c - \omega \mathbf{D} \cdot \nabla c) - q_c = 0 \quad \text{over } \Omega \text{ and }]0, T] \quad (\text{A1})$$

716 with initial and boundary conditions:

$$717 \quad \begin{cases} c = c^0 & \text{over } \Omega \text{ at } t = 0 \\ c = c_D & \text{over } \partial_D \Omega_C \text{ and }]0, T] \\ -\mathbf{D} \cdot \nabla c \cdot \mathbf{n}_\Gamma = q_N^c & \text{over } \partial_N \Omega_C \text{ and }]0, T] \end{cases} \quad (\text{A2})$$

718 At this stage, perturbations $\delta \mathbf{p}$ resulting in perturbations δc to keep $\mathcal{V}(c + \delta c, \mathbf{p} + \delta \mathbf{p}) = 0$
 719 only concern model parameters, that is, $\delta \mathbf{p} = (\delta \omega, \delta \mathbf{u}, \delta \mathbf{D})$, noting that \mathbf{u} is a parameter for the
 720 transport equation but also an output of a flow model. A later discussion will address
 721 perturbations regarding source/sink terms, initial conditions, and boundary conditions. A
 722 variation of the Lagrangian operator is employed to derive the equations of the adjoint state,
 723 which takes the form:

$$724 \quad \delta \mathcal{L} = \int_0^T \int_\Omega \frac{\partial f}{\partial c} \delta c \, d\Omega dt + \int_0^T \int_\Omega \frac{\partial f}{\partial \mathbf{p}} \delta \mathbf{p} \, d\Omega dt + \int_0^T \int_\Omega (\mathcal{V}(c + \delta c, \mathbf{p} + \delta \mathbf{p}) - \mathcal{V}(c, \mathbf{p})) \mu \, d\Omega dt$$

725 (A3)

726 with f the continuous objective function, μ the continuous adjoint state, and the constraint
 727 $\mathcal{V}(c + \delta c, \mathbf{p} + \delta \mathbf{p}) = 0$. The latter is developed as:

$$\begin{aligned}
728 \quad \mathcal{V}(c + \delta c, \mathbf{p} + \delta \mathbf{p}) = 0 &\equiv \frac{\partial(\omega + \delta\omega)(c + \delta c)}{\partial t} + \nabla \cdot ((\omega + \delta\omega)(\mathbf{u} + \delta\mathbf{u})(c + \delta c)) \\
&\quad - \nabla \cdot ((\omega + \delta\omega)(\mathbf{D} + \delta\mathbf{D}) \cdot \nabla(c + \delta c)) - q_c = 0 \quad \text{over } \Omega \text{ and }]0, T] \quad (A4)
\end{aligned}$$

729 and flanked with initial and boundary conditions:

$$730 \quad \begin{cases} c + \delta c = c^0 & \text{over } \Omega \text{ at } t = 0 \\ c + \delta c = c_D & \text{over } \partial_D \Omega_C \text{ and }]0, T] \\ -(\mathbf{D} + \delta\mathbf{D}) \nabla(c + \delta c) \cdot \mathbf{n}_\Gamma = q_N^C & \text{over } \partial_N \Omega_C \text{ and }]0, T] \end{cases} \quad (A5)$$

731 Developing to the first order (i.e., by neglecting terms in δ^2), the difference $\mathcal{V}_\delta - \mathcal{V}$ renders:

$$\begin{aligned}
732 \quad \mathcal{V}(c + \delta c, \mathbf{p} + \delta \mathbf{p}) - \mathcal{V}(c, \mathbf{p}) = 0 &\equiv \\
&\frac{\partial(\omega\delta c)}{\partial t} + \frac{\partial(c\delta\omega)}{\partial t} + \nabla \cdot (\omega\mathbf{u}\delta c) + \nabla \cdot (\omega\delta\mathbf{u}c) + \nabla \cdot (\delta\omega\mathbf{u}c) \\
&\quad - \nabla \cdot (\omega\mathbf{D}\nabla\delta c) - \nabla \cdot (\omega\delta\mathbf{D}\nabla c) - \nabla \cdot (\delta\omega\mathbf{D}\nabla c) = 0 \quad \text{over } \Omega \text{ and }]0, T] \quad (A6)
\end{aligned}$$

733 with initial and boundary conditions:

$$734 \quad \begin{cases} \delta c = 0 & \text{over } \Omega \text{ at } t = 0 \\ \delta c = 0 & \text{over } \partial_D \Omega_C \text{ and }]0, T] \\ -\mathbf{D} \cdot \nabla \delta c \cdot \mathbf{n}_\Gamma - \delta\mathbf{D} \cdot \nabla c \cdot \mathbf{n}_\Gamma = 0 & \text{over } \partial_N \Omega_C \text{ and }]0, T] \end{cases} \quad (A7)$$

735 The basic idea prevailing for the identification of the continuous adjoint state equations

736 is to isolate the terms in δ in the integrals $\int_0^T \int_\Omega (\mathcal{V}_\delta - \mathcal{V}) \mu d\Omega dt$ of the operator $\delta\mathcal{L}$ in Eq.

737 (A3). This occurs via integration by parts for all terms in Eq. (A6), which are handled below as

738 they appear ranked in Eq. (A6).

$$\begin{aligned}
739 \quad \int_0^T \int_\Omega \frac{\partial(\omega\delta c)}{\partial t} \mu d\Omega dt &= - \int_0^T \int_\Omega \omega\delta c \frac{\partial\mu}{\partial t} d\Omega dt + \left[\int_\Omega \omega\delta c \mu d\Omega \right]_0^T \\
&= - \int_0^T \int_\Omega \omega\delta c \frac{\partial\mu}{\partial t} d\Omega dt \quad (A8)
\end{aligned}$$

740 In Eq. (A8), simplifications come from the following properties: at $t=0$, $\delta c = 0$ is due to

741 boundary conditions in Eq. (A7); at $t=T$, μ is set to zero as it is the initial condition for

742 calculating μ (see below), and μ can be defined up to the addition of a constant.

$$\begin{aligned}
743 \quad \int_0^T \int_{\Omega} \frac{\partial(c\delta\omega)}{\partial t} \mu d\Omega dt &= - \int_0^T \int_{\Omega} c\delta\omega \frac{\partial\mu}{\partial t} d\Omega dt + \left[\int_{\Omega} c\delta\omega\mu d\Omega \right]_0^T \\
&= - \int_0^T \int_{\Omega} c\delta\omega \frac{\partial\mu}{\partial t} d\Omega dt - \int_{\Omega} c^0 \delta\omega^0 \mu^0 d\Omega
\end{aligned} \tag{A9}$$

744 where it has been accounted for the fact that $\mu = 0$ at $t = T$. We note that:

$$745 \quad \int_0^T \frac{\partial a}{\partial t} b dt = - \int_0^T \frac{\partial b}{\partial t} a dt + [a b]_0^T = - \int_0^T \frac{\partial b}{\partial t} a dt - a^0 b^0 \text{ if } b^T = 0 \tag{A10}$$

746 Using the property $\mu = 0$ at $t = T$ and applying Eq. (A10) in Eq. (A9) results in:

$$747 \quad \int_0^T \int_{\Omega} \frac{\partial(c\delta\omega)}{\partial t} \mu d\Omega dt = \int_0^T \int_{\Omega} \delta\omega\mu \frac{\partial c}{\partial t} d\Omega dt \tag{A11}$$

$$748 \quad \int_0^T \int_{\Omega} \nabla \cdot (\omega \mathbf{u} \delta c) \mu d\Omega dt = - \int_0^T \int_{\Omega} \omega \delta c \mathbf{u} \cdot \nabla \mu d\Omega dt + \int_0^T \int_{\partial_N \Omega_c} \omega \delta c \mu \mathbf{u} \cdot \mathbf{n}_{\Gamma} d\Gamma dt \tag{A12}$$

749 In Eq. (A12), the contour integral over the Dirichlet-type boundary $\partial_D \Omega_c$ has been cancelled

750 out, considering that $\delta c = 0$ along this type of boundary (see Eq. (A7)).

$$\begin{aligned}
751 \quad \int_0^T \int_{\Omega} \nabla \cdot (\omega \delta \mathbf{u} c) \mu d\Omega dt &= - \int_0^T \int_{\Omega} \omega c \delta \mathbf{u} \cdot \nabla \mu d\Omega dt + \int_0^T \int_{\partial \Omega} \omega c \mu \delta \mathbf{u} \cdot \mathbf{n}_{\Gamma} d\Gamma dt \\
&= - \int_0^T \int_{\Omega} \omega c \delta \mathbf{u} \cdot \nabla \mu d\Omega dt
\end{aligned} \tag{A13}$$

$$\begin{aligned}
752 \quad \int_0^T \int_{\Omega} \nabla \cdot (\delta \omega \mathbf{u} c) \mu d\Omega dt &= - \int_0^T \int_{\Omega} \delta \omega c \mathbf{u} \cdot \nabla \mu d\Omega dt + \int_0^T \int_{\partial \Omega} \delta \omega c \mu \mathbf{u} \cdot \mathbf{n}_{\Gamma} d\Gamma dt \\
&= - \int_0^T \int_{\Omega} \delta \omega c \mathbf{u} \cdot \nabla \mu d\Omega dt
\end{aligned} \tag{A14}$$

753 In Eqs. (A13) and (A14), the contour integrals cancel out because the perturbations $\delta \mathbf{u}$ and

754 $\delta \omega$ are null along the boundaries (ω and \mathbf{u} are not defined straight at the boundary of the

755 modeled domain, they do not appear in the boundary conditions), and incidentally, the adjoint

756 state μ , which is defined up to the addition of a constant, can be considered as null along a

757 Dirichlet-type boundary.

$$\begin{aligned}
& -\int_0^T \int_{\Omega} \nabla \cdot (\omega \mathbf{D} \cdot \nabla \delta c) \mu \, d\Omega dt = -\int_0^T \int_{\Omega} \delta c \nabla \cdot (\omega \mathbf{D} \cdot \nabla \mu) \, d\Omega dt + \int_0^T \int_{\partial\Omega} \delta c \omega \mathbf{D} \cdot \nabla \mu \cdot \mathbf{n}_{\Gamma} \, d\Gamma dt \\
& -\int_0^T \int_{\partial\Omega} \omega \mu \mathbf{D} \cdot \nabla \delta c \cdot \mathbf{n}_{\Gamma} \, d\Gamma dt \\
& = -\int_0^T \int_{\Omega} \delta c \nabla \cdot (\omega \mathbf{D} \cdot \nabla \mu) \, d\Omega dt + \int_0^T \int_{\partial_N \Omega_c} \delta c \omega \mathbf{D} \cdot \nabla \mu \cdot \mathbf{n}_{\Gamma} \, d\Gamma dt
\end{aligned} \tag{A15}$$

758 The expression in Eq. (A15) has been integrated by parts twice to extract the perturbation δc
760 from the operator $\nabla \cdot \nabla$. The simplification of contour integrals results from $\mu = 0$ over the
761 contour $\partial_D \Omega_c$, and the boundary conditions $\delta c = 0$ over $\partial_D \Omega_c$. Note also that $\mathbf{D} \cdot \nabla \delta c \cdot \mathbf{n}_{\Gamma}$ from
762 (A15) in addition to $\delta \mathbf{D} \cdot \nabla c \cdot \mathbf{n}_{\Gamma}$ which appear in (A16) results in a null term over $\partial_N \Omega_c$ (see
763 boundary conditions (A7)).

$$\begin{aligned}
& -\int_0^T \int_{\Omega} \nabla \cdot (\omega \delta \mathbf{D} \cdot \nabla c) \mu \, d\Omega dt = \int_0^T \int_{\Omega} \omega (\nabla \mu)^T \cdot \delta \mathbf{D} \cdot \nabla c \, d\Omega dt - \int_0^T \int_{\partial\Omega} \omega \mu \delta \mathbf{D} \cdot \nabla c \cdot \mathbf{n}_{\Gamma} \, d\Gamma dt \\
& = \int_0^T \int_{\Omega} \omega (\nabla \mu)^T \cdot \delta \mathbf{D} \cdot \nabla c \, d\Omega dt
\end{aligned} \tag{A16}$$

765 In Eq (A16) the contour integral cancels out because $\mu = 0$ over the contour $\partial_D \Omega_c$, and
766 $\delta \mathbf{D} \cdot \nabla c \cdot \mathbf{n}_{\Gamma}$ in addition to $\mathbf{D} \cdot \nabla \delta c \cdot \mathbf{n}_{\Gamma}$ in (A15) cancel out over $\partial_N \Omega_c$.

$$\begin{aligned}
& -\int_0^T \int_{\Omega} \nabla \cdot (\delta \omega \mathbf{D} \cdot \nabla c) \mu \, d\Omega dt = \int_0^T \int_{\Omega} \delta \omega (\nabla \mu)^T \cdot \mathbf{D} \cdot \nabla c \, d\Omega dt - \int_0^T \int_{\partial\Omega} \delta \omega \mu \mathbf{D} \cdot \nabla c \cdot \mathbf{n}_{\Gamma} \, d\Gamma dt \\
& = \int_0^T \int_{\Omega} \delta \omega (\nabla \mu)^T \cdot \mathbf{D} \cdot \nabla c \, d\Omega dt
\end{aligned} \tag{A17}$$

768 In Eq (A17), the contour integral cancels out because $\mu = 0$ over the contour $\partial_D \Omega_c$, and the
769 perturbation $\delta \omega$ is zero over the whole contour $\partial\Omega$.

770 Gathering all terms in δc over the expressions in Eqs. (A8) to (A17), then reintroducing
 771 them into the variation of the Lagrangian operator $\delta \mathcal{L}$ in Eq. (A3) and cancelling out the
 772 whole, poses the continuous equations of the adjoint state, which render:

$$773 \begin{cases} -\omega \frac{\partial \mu}{\partial t} - \omega \mathbf{u} \cdot \nabla \mu - \nabla \cdot (\omega \mathbf{D} \cdot \nabla \mu) + \frac{\partial f}{\partial c} = 0 & \text{over } \Omega \text{ and }]T,0] \\ \mu = 0 & \text{over } \Omega \text{ at } t = T \\ \mu = 0 & \text{over } \partial_D \Omega_C \text{ and }]T,0] \\ (\omega \mu \mathbf{u} + \omega \mathbf{D} \cdot \nabla \mu) \cdot \mathbf{n}_\Gamma = 0 & \text{over } \partial_N \Omega_C \text{ and }]T,0] \end{cases} \quad (\text{A18})$$

774 It is worth noting that Eq. (A18) has to be solved backward in time and with a reversed velocity
 775 field $-\mathbf{u}$; otherwise, the problem lacks physical meaning with a negative dispersion tensor in
 776 the advection-dispersion equation. The Neumann boundary condition of the forward problem
 777 in Eq. (A2) has been transformed into a Robin boundary condition (with a reversed velocity
 778 field $-\mathbf{u}$) along the contour $\partial_N \Omega_C$. Usually in transport problems, a so-called homogeneous
 779 Neumann boundary condition $-\mathbf{D} \nabla c \cdot \mathbf{n}_\Gamma = 0$ is associated with a no-flow boundary, yielding
 780 $\mathbf{u} \cdot \mathbf{n}_\Gamma = 0$. In that case, the Robin boundary condition for the adjoint state simplifies into
 781 $\nabla \mu \cdot \mathbf{n}_\Gamma = 0$. Another possibility where the condition $-\mathbf{D} \nabla c \cdot \mathbf{n}_\Gamma = 0$ applies is that of a "free"
 782 advective flux exiting the system with no modification beyond the boundary. In that case, the
 783 Robin boundary condition of the adjoint state with a reversed flow field simply consists in
 784 letting a prescribed value $\mu = 0$ enter into the domain.

785 Solving the adjoint state equations in Eq. (A18) changes the expression of the variation
 786 of the Lagrangian operator in Eq. (A3), which simplifies into:

$$787 \delta \mathcal{L} = \int_0^T \int_\Omega \frac{\partial f}{\partial \mathbf{p}} \delta \mathbf{p} d\Omega dt + \int_0^T \int_\Omega \delta \mathbf{p} \mathcal{G}(c, \mu) d\Omega dt \quad (\text{A19})$$

788 With the three types of parameters ω , \mathbf{u} , and \mathbf{D} in \mathbf{p} , the operator $\delta \mathcal{L}$ can be separated into
 789 three components:

790 From Eqs. (A11), (A14), and (A17):

$$791 \quad \delta\mathcal{L}|_{\omega} = \int_0^T \int_{\Omega} \delta\omega \frac{\partial f}{\partial \omega} d\Omega dt + \int_0^T \int_{\Omega} \delta\omega \left(\frac{\partial c}{\partial t} \mu - c \mathbf{u} \cdot \nabla \mu + (\nabla \mu)^T \cdot \mathbf{D} \cdot \nabla c \right) d\Omega dt \quad (\text{A20})$$

792 From Eq. (A13):

$$793 \quad \delta\mathcal{L}|_{\mathbf{u}} = \int_0^T \int_{\Omega} \delta \mathbf{u} \frac{\partial f}{\partial \mathbf{u}} d\Omega dt - \int_0^T \int_{\Omega} \omega c \delta \mathbf{u} \cdot \nabla \mu d\Omega dt \quad (\text{A21})$$

794 From Eq. (A16):

$$795 \quad \delta\mathcal{L}|_{\mathbf{D}} = \int_0^T \int_{\Omega} \delta \mathbf{D} \frac{\partial f}{\partial \mathbf{D}} d\Omega dt + \int_0^T \int_{\Omega} \omega (\nabla \mu)^T \cdot \delta \mathbf{D} \cdot \nabla c d\Omega dt \quad (\text{A22})$$

796 The expressions in Eqs. (A20), (A21), and (A22) give the form of the gradient components of

797 the objective function with respect to parameters ω , \mathbf{u} , and \mathbf{D} . For example, let us take $u_{x,i}^n$,

798 the velocity along the x direction over a subdomain Ω_i of Ω and over the time step Δt_n within

799 the period $]0, T]$. The gradient component of the objective function with respect to $u_{x,i}^n$ is

800 expressed via Eq. (A21) as:

$$801 \quad \frac{dF}{\delta u_{x,i}^n} \approx \frac{\delta \mathcal{L}}{\delta u_{x,i}^n} = \int_{\Delta t_n} \int_{\Omega_i} \frac{\partial f}{\partial u_{x,i}^n} d\Omega dt - \int_{\Delta t_n} \int_{\Omega_i} \omega c \frac{\partial \mu}{\partial x} d\Omega dt \quad (\text{A23})$$

802 The strength of the continuous adjoint state also allows us to retrieve source/sink terms,

803 initial conditions, and boundary conditions by providing the gradient components of the

804 objective function with respect to these factors. Regarding source/sink terms, the operator

805 $\mathcal{V}_{\delta} - \mathcal{V}$ in Eq. (A6) is modified to include a perturbation $-\delta q_c$. As this perturbation is

806 independent of that on the parameters $\delta\omega$, $\delta\mathbf{u}$, and $\delta\mathbf{D}$, the integration $\int_0^T \int_{\Omega} (\mathcal{V}_{\delta} - \mathcal{V}) \mu d\Omega dt$

807 simply lets an additional term in the form $-\int_0^T \int_{\Omega} \delta q_c \mu d\Omega dt$ appear. The latter does not alter the

808 development between Eqs. (A8) and (A17). Consequently, the continuous adjoint state equation

809 (A18) and the gradient components of the objective function (precisely, the components of the
810 operator $\delta\mathcal{L}$) with respect to parameters $\boldsymbol{\omega}$, \mathbf{u} , and \mathbf{D} (Eqs. A20, A21, and A22) are
811 unmodified. After the adjoint state μ has been calculated by solving Eq. (A18), the gradient
812 components of the objective function with respect to source/sink terms q_c are calculated by
813 employing:

$$814 \quad \delta\mathcal{L}|_{q_c} = \int_0^T \int_{\Omega} \delta q_c \frac{\partial f}{\partial q_c} d\Omega dt - \int_0^T \int_{\Omega} \delta q_c \mu d\Omega dt \quad (\text{A24})$$

815 Regarding initial and boundary conditions, the operator $\mathcal{V}_{\delta} - \mathcal{V}$ in (A6) is modified on
816 its initial and boundary conditions in Eq. (A7). The latter become:

$$817 \quad \begin{cases} \delta c = \delta c^0 & \text{over } \Omega \text{ at } t = 0 \\ \delta c = \delta c_D & \text{over } \partial_D \Omega_C \text{ and }]0, T] \\ -\mathbf{D} \cdot \nabla \delta c \cdot \mathbf{n}_{\Gamma} - \delta \mathbf{D} \cdot \nabla c \cdot \mathbf{n}_{\Gamma} = \delta q_N^c & \text{over } \partial_N \Omega_C \text{ and }]0, T] \end{cases} \quad (\text{A25})$$

818 with δc^0 the perturbation associated with initial conditions, and δc_D , δq_N^c the perturbations
819 associated with Dirichlet- and Neumann-type boundary conditions, respectively. The general

820 form of the operator $\int_0^T \int_{\Omega} (\mathcal{V}_{\delta} - \mathcal{V}) \mu d\Omega dt$ is not modified, but the expansion of a few terms

821 slightly changes. δc^0 appears in Eq. (A8), which becomes:

$$822 \quad \begin{aligned} \int_0^T \int_{\Omega} \frac{\partial \omega \delta c}{\partial t} \mu d\Omega dt &= - \int_0^T \int_{\Omega} \omega \delta c \frac{\partial \mu}{\partial t} d\Omega dt + \left[\int_{\Omega} \omega \delta c \mu d\Omega \right]_0^T \\ &= - \int_0^T \int_{\Omega} \omega \delta c \frac{\partial \mu}{\partial t} d\Omega dt + \int_{\Omega} \omega \delta c^0 \mu^0 d\Omega \end{aligned} \quad (\text{A26})$$

823 where the properties $\mu = 0$ at $t = T$ and $\delta c = \delta c^0$ at $t = 0$ have been accounted for. The
824 perturbations δc_D and δq_N^c appear in the two successive integrations by parts of Eq. (A15) and
825 the integration by parts of (A16). More precisely, only the contour integrals are modified; their
826 sum from expressions in (A15) and (A16) renders:

$$\begin{aligned}
& \int_0^T \int_{\partial\Omega} \delta c \omega \mathbf{D} \cdot \nabla \mu \cdot \mathbf{n}_\Gamma \, d\Gamma dt - \int_0^T \int_{\partial\Omega} \omega \mu \mathbf{D} \cdot \nabla \delta c \cdot \mathbf{n}_\Gamma \, d\Gamma dt \\
& \quad - \int_0^T \int_{\partial\Omega} \omega \mu \delta \mathbf{D} \cdot \nabla c \cdot \mathbf{n}_\Gamma \, d\Gamma dt \\
827 \quad & = \int_0^T \int_{\partial_N \Omega_c} \delta c \omega \mathbf{D} \cdot \nabla \mu \cdot \mathbf{n}_\Gamma \, d\Gamma dt + \int_0^T \int_{\partial_D \Omega_c} \delta c_D \omega \mathbf{D} \cdot \nabla \mu \cdot \mathbf{n}_\Gamma \, d\Gamma dt \quad (\text{A27}) \\
& \quad + \int_0^T \int_{\partial_N \Omega_c} \omega \mu \delta q_N^c \cdot \mathbf{n}_\Gamma \, d\Gamma dt
\end{aligned}$$

828 The contour integrals of Eq. (A27) take into account the following properties: $\mu = 0$ over the
829 contour $\partial_D \Omega_c$, the boundary condition $\delta c = \delta c_D$ over $\partial_D \Omega_c$, and the boundary condition
830 $-\mathbf{D} \cdot \nabla \delta c \cdot \mathbf{n}_\Gamma - \delta \mathbf{D} \cdot \nabla c \cdot \mathbf{n}_\Gamma = \delta q_N^c$ over $\partial_N \Omega_c$.

831 All the remaining terms in the development of $\int_0^T \int_{\Omega} (\mathcal{V}_\delta - \mathcal{V}) \mu \, d\Omega dt$ are unchanged,
832 which also comes down to unchanged continuous equations for the adjoint state μ and the
833 components of Lagrangian operator $\delta \mathcal{L}$ regarding perturbations on parameters $\delta \omega$, $\delta \mathbf{u}$, and
834 $\delta \mathbf{D}$. When the adjoint state has been calculated by solving Eq. (A18), the gradient components
835 of the objective function with respect to initial and boundary conditions are accessible via:

$$\begin{aligned}
& \delta \mathcal{L}|_{c^0} = \int_0^T \int_{\Omega} \delta c^0 \frac{\partial f}{\partial c^0} \, d\Omega dt + \int_{\Omega} \delta c^0 \omega \mu^0 \, d\Omega \\
836 \quad & \delta \mathcal{L}|_{c_D} = \int_0^T \int_{\partial_D \Omega_c} \delta c_D \frac{\partial f}{\partial c_D} \, d\Omega dt + \int_0^T \int_{\partial_D \Omega_c} \delta c_D \omega \mathbf{D} \cdot \nabla \mu \cdot \mathbf{n}_\Gamma \, d\Gamma dt \quad (\text{A28}) \\
& \delta \mathcal{L}|_{q_N^c} = \int_0^T \int_{\partial_N \Omega_c} \delta q_N^c \frac{\partial f}{\partial q_N^c} \, d\Omega dt + \int_0^T \int_{\partial_N \Omega_c} \omega \mu \delta q_N^c \cdot \mathbf{n}_\Gamma \, d\Gamma dt
\end{aligned}$$

837

838 **References**

839

840 Ackerer, P., Delay, F., 2010. Inversion of a set of well-test interferences in a fractured limestone
841 aquifer by using an automatic downscaling parameterization technique. *J. Hydrol.* 389, 42–56.
842 <https://doi.org/10.1016/j.jhydrol.2010.05.020>.

843

844 Ackerer, P., Trottier, N., Delay, F., 2014. Flow in double-porosity aquifers: Parameter
845 estimation using an adaptive multiscale method. *Adv. Water Resour.* 73, 108–122.
846 <https://doi.org/10.1016/j.advwatres.2014.07.001>.

847

848 Bear, J., 1972. *Dynamics of Fluids in Porous Media*. Elsevier Publications. 335 p.

849

850 Bertsekas, D.P., 1996. *Constrained optimization and Lagrange multiplier methods*. Athena
851 Scientific, Belmont-Massachusetts.

852

853 Byrd, R.H., Lu, L., Nocedal, J., Zhu, C. A limited memory algorithm for bound constraint
854 optimization. Northwest Univ, Dpt Electrical Eng Computer Science, Tech Rep, NAM-08;
855 1994.

856

857 Carniato, L., Schoups, G., van de Giesena, N., Seuntjens, P., Bastiaens, L., Sapione H., 2015.
858 Highly parameterized inversion of groundwater reactive transport for a complex field site.
859 *Journal of Contaminant Hydrology*, 173, 38–58
860 <http://dx.doi.org/10.1016/j.jconhyd.2014.12.001>.

861

862 Carrera, J., Neuman, S.P., 1986. Estimation of Aquifer Parameters Under Transient and Steady
863 State Conditions: 1. Maximum Likelihood Method Incorporating Prior Information. *Water*
864 *Resour. Res.* 22, 199–210. <https://doi.org/10.1029/WR022i002p00199>.

865

866 Chavent, G., 1979. Identification of distributed parameter system: about the output least square
867 method, its implementation and identification. In *Identification and System Parameter*
868 *Estimation*, R. Isermann, Ed., vol.1, pp.85–97, Pergamon Press, New York, USA, 1979.

869

870 Cooley, R.L., 1985. A comparison of several methods of solving nonlinear-regression
871 groundwater-flow problems. *Water Resour. Res.* 21 (10), 1525–1538.

872

873 Delay, F., Badri, H., Fahs, M., Ackerer, P., 2017. A comparison of discrete versus continuous
874 adjoint states to invert groundwater flow in heterogeneous dual porosity systems. *Adv. Water*
875 *Resour.* 110, 1–18. <https://doi.org/10.1016/j.advwatres.2017.09.022>.

876

877 Deng, C., Liu, P., Guo, S., Li, Z., Wang, D., 2016. Identification of hydrological model
878 parameter variations using ensemble Kalman filter. *Hydrol. Earth Syst. Sci.* 20, 4949–4961.
879 <https://doi.org/10.5194/hess-20-4949-2016>.

880

881 Doherty, J., 2003. Ground Water model calibration using pilot points and regularization.
882 *Groundwater* 41, 170–177. <https://doi.org/10.1111/j.1745-6584.2003.tb02580.x>

883

884 Emsellem, Y., de Marsily, G., 1971. An automatic solution of the inverse problem. *Water*
885 *Resour. Res.* 7 (5), 1264–1283.

886

887 Erdal, D., Cirpka, O.A., 2017. Preconditioning an ensemble Kalman filter for groundwater flow
888 using environmental-tracer observations. *J. Hydrol.* 545, 42–54.
889 <http://dx.doi.org/10.1016/j.jhydrol.2016.11.064>,
890

891 Giudici, M., Vassena, C., 2008. Spectral analysis of the balance equation of groundwater
892 hydrology. *Transport Porous Med.* 72 (2), 171–178. [https://doi.org/10.1007/s11242-007-9142-](https://doi.org/10.1007/s11242-007-9142-3)
893 3.
894

895 Hassane, F., Ackerer, P., 2017. Groundwater flow parameter estimation using refinement and
896 coarsening indicators for adaptive downscaling parameterization. *Adv. Water Resour.* 100,
897 139–152. <https://doi.org/10.1016/j.advwatres.2016.12.013>.
898

899 Hassane, F.M., Ackerer, P., Younes, A., Guadagnini, A., Berkowitz, B., 2017. Benchmarking
900 numerical codes for tracer transport with the aid of laboratory-scale experiments in 2D
901 heterogeneous porous media. *J. Contam. Hydrol.*
902 <https://doi.org/10.1016/j.jconhyd.2017.06.001>.
903

904 Hendricks Franssen, H-J., Alcolea, A., Riva, M., Bakr, M., van der Wiel, N., Stauffer, F.,
905 Guadagnini, A., 2009. A comparison of seven methods for the inverse modelling of
906 groundwater flow. Application to the characterization of well catchments. *Adv. Water Resour.*
907 32, 851–872. <https://doi.org/10.1016/j.advwatres.2009.02.011>.
908

909 Hendricks Franssen, H-J., Gomez-Hernandez, J., Sahuquillo, A. 2003. Coupled inverse
910 modelling of groundwater flow and mass transport and the worth of concentration data, *J.*
911 *Hydrol.* 281, 281–295, [doi:10.1016/S0022-1694\(03\)00191-4](https://doi.org/10.1016/S0022-1694(03)00191-4).
912

913 Iglesias, M.A., Law, K.J.H., Stuart, A.M., 2013. Ensemble Kalman methods for inverse
914 problems. *Inverse Probl.* 29, 045001. <https://doi.org/10.1088/0266-5611/29/4/045001>.
915

916 Kalman, R.E., 1960. A new approach to linear filtering and prediction problems. *T. Am. Math.*
917 *Soc.* 82 (D), 35-45.
918

919 Keidser, A., Rosbjerg, D., 1991. A comparison of four inverse approaches to groundwater flow
920 and transport parameter identification. *Water Resour. Res.* 27. [doi: 10.1029/91WR00990](https://doi.org/10.1029/91WR00990). issn:
921 0043-1397.
922

923 Kitanidis, P.K., Lee, J., 2014. Principal Component Geostatistical Approach for large-
924 dimensional inverse problems. *Water Resour. Res.* 50, 5428–5443.
925 <https://doi.org/10.1002/2013WR014630>.
926

927 Levenberg, K., 1944. A Method for the solution of certain non-linear problems in least Squares.
928 *Q. Appl. Math.* 2, 164–168.
929

930 Li, L., Zhou, H., Gomez-Hernandez, J.J., Hendricks Franssen, H-J. 2012. Jointly mapping
931 hydraulic conductivity and porosity by assimilating concentration data via ensemble Kalman
932 filter. *J. Hydrol.* 428–429, 152–169. <http://dx.doi.org/10.1016/j.jhydrol.2012.01.037>.
933

934 Linde, N., Renard, P., Mukerji, T., Caers, J., 2015. Geological realism in hydrogeological and
935 geophysical inverse modeling: A review. *Adv. Water Resour.* 86, 86–101.
936 <https://doi.org/10.1016/j.advwatres.2015.09.019>.

937
938 Liu, G., Chen, Y., Zhang, D., 2008. Investigation of flow and transport process at the MADE
939 site using ensemble Kalman filter. *Adv. Water Resour.* 31, 975–986.
940 <http://dx.doi.org/10.1016/j.advwatres.2008.03.006>.
941
942 Marquardt, D.W., 1963. An algorithm for least-squares estimation of nonlinear parameters. *J.*
943 *Soc. Ind. Appl. Math.* 11 (2), 431-441.
944
945 Medina, A., Carrera, J., 1996. Coupled estimation of flow and solute transport parameters.
946 *Water Resour. Res.* 32 (10), 3063-3076. [DOI.10.1029/96WR00754](https://doi.org/10.1029/96WR00754).
947
948 Medina, A., Carrera, J., 2003. Geostatistical inversion of coupled problems: dealing with
949 computational burden and different types of data. *J. Hydrol.* 281, 251–264.
950 [https://doi.org/10.1016/S0022-1694\(03\)00190-2](https://doi.org/10.1016/S0022-1694(03)00190-2).
951
952 Neuman, S.P., Carrera, J., 1985. Maximum-likelihood adjoint-state finite-element estimation
953 of groundwater parameters under steady- and nonsteady-state conditions. *Appl. Math. Comput.*
954 17, 405–432. [https://doi.org/10.1016/0096-3003\(85\)90043-8](https://doi.org/10.1016/0096-3003(85)90043-8).
955
956 Pollock D., Cirpka, O.A., 2012. Fully coupled hydrogeophysical inversion of a laboratory salt
957 tracer experiment monitored by electrical resistivity tomography. *Water Res. Res.* 48, W01505,
958 [doi:10.1029/2011WR010779](https://doi.org/10.1029/2011WR010779).
959
960 Pool, M., Carrera, J., Alcolea, A., Bocanegra, E.M., 2015. A comparison of deterministic and
961 stochastic approaches for regional scale inverse modeling on the Mar del Plata aquifer. *J.*
962 *Hydrol.* 531, 214–229. <https://doi.org/10.1016/j.jhydrol.2015.09.064>.
963
964 Sun, N-Z., 1994. *Inverse Problems in Groundwater Modeling*, Kluwer Academic Publishers,
965 Dordrecht.
966
967 Sun, N-Z., Sun, A., 2015. *Model Calibration and Parameter Estimation*. Springer New York,
968 New York, NY. <https://doi.org/10.1007/978-1-4939-2323-6>.
969
970 Sun, N-Z., Yeh, W.W-G., 1990. Coupled inverse problems in groundwater modeling: 1.
971 Sensitivity analysis and parameter identification. *Water Resour. Res.* 26, 2507–2525.
972 <https://doi.org/10.1029/WR026i010p02507>
973
974 Strecker, E.W., Chu, W., 1986. Parameter identification of a ground water contaminant transport
975 model. *Groundwater* 24, 56–62. <https://doi.org/10.1111/j.1745-6584.1986.tb01459.x>
976
977 Umari, A., Willis, R., Liu, P.L-F., 1979. Identification of aquifer dispersivities in two-
978 dimensional transient groundwater contaminant transport: An optimization approach. *Water*
979 *Resour Res.* 15, 815–831. <https://doi.org/10.1029/WR015i004p00815>
980
981 Vemuri, V., Dracup, J.A., Erdmann, R.C., 1969. Sensitivity analysis method of system
982 identification and its potential in hydrologic research. *Water Resour. Res.* 5 (2), 341-349.
983
984 Wagner, B.J., Gorelick, S.M., 1987. Optimal groundwater quality management under parameter
985 uncertainty. *Water Resour. Res.* 23, 1162–1174. <https://doi.org/10.1029/WR023i007p01162>

986
987 Wagner, B.J., 1992. Simultaneous parameter estimation and contaminant source
988 characterization for coupled groundwater flow and contaminant transport modelling. *J. Hydrol.*
989 135, 275–303. [https://doi.org/10.1016/0022-1694\(92\)90092-A](https://doi.org/10.1016/0022-1694(92)90092-A)
990
991 Wen, X-H., Deutsch, C.V., Cullick, A.S., 2002. Construction of geostatistical aquifer models
992 integrating dynamic flow and tracer data using inverse technique. *J. Hydrol.* 255, 151–168.
993
994 Yeh, W.W.G., Tauxe, G.W., 1971. Quasi-linearization and the identification of aquifer
995 parameters. *Water Resour. Res.* 7 (2), 375-381.
996
997 Younes, A., Ackerer, P., Delay, F., 2010. Mixed finite elements for solving 2-D diffusion-type
998 equations, *Rev. Geophys.*, 48, RG1004, [doi:10.1029/2008RG000277](https://doi.org/10.1029/2008RG000277).
999
1000 Zhou, H., Gómez-Hernández, J.J., Li, L., 2014. Inverse methods in hydrogeology: Evolution
1001 and recent trends. *Adv. Water Resour.* 63, 22–37.
1002 <https://doi.org/10.1016/j.advwatres.2013.10.014>.
1003
1004

1005 **Figure and table captions**

1006

1007 **Fig. 1.** Flow domains of the three synthetic test cases C1, C2, and C3. Dirichlet boundary
1008 conditions for flow at western (red bolt line, $h = 100$ m) and eastern (blue bolt line, $h = 90$ m)
1009 boundaries. North and south boundaries are of no-flow type. Green lines in test cases C1 and
1010 C2 delimit the boundary associated with continuous uniform injection of solute. The green
1011 rectangle in test case C3 is the location of a short-step injection of solute. Observations of
1012 hydraulic heads and concentrations are located at the square dots. Blue and red dots mark the
1013 locations of extraction and injection wells, respectively. Wells P7, P9, and P11 are locations
1014 where solute concentration breakthrough curves are compared between reference and inverse
1015 solutions.

1016 **Fig. 2.** Reference log hydraulic conductivity ($\log K$) and porosity (ω) fields.

1017 **Fig. 3.** Reference and examples of simulated head fields (constant over time) and solute plumes
1018 after 120 days for flow and transport test case C1, 80 days for test case C2, and 50 days for test
1019 case C3. S1, S2, and S3 denote the strategies employed for inversion, and h or c refer to either
1020 head or concentration fields. Black lines through some fields mark the main streamlines of the
1021 flow field. The reference flow fields for test cases C2 and C3 are similar. The color scale ranks
1022 values for both head and concentration casted between 0 and 1 for minimal and maximal
1023 reference values, respectively

1024 **Fig. 4.** Solute concentration breakthrough curves at the three locations P11, P7, and P9 (ranked
1025 with increasing distance from solute source) for test case C1 and three inversion strategies S1,
1026 S2, and S3. Black lines denote the references; blue areas delineate the envelope $[\langle c \rangle \pm \sigma_c]$ of
1027 50 inverse solutions.

1028 **Fig. 5.** Solute concentration breakthrough curves at the three locations P11, P7, and P9 (ranked
1029 with increasing distance from solute source) for test case C2 and three inversion strategies S1,
1030 S2, and S3. Black lines denote the references; blue areas delineate the envelope $[\langle c \rangle \pm \sigma_c]$ of
1031 50 inverse solutions.

1032 **Fig. 6.** Solute concentration breakthrough curves at the three locations P11, P7, and P9 (ranked
1033 with increasing distance from solute source) for test case C3 and three inversion strategies S1,
1034 S2, and S3. Black lines denote the references; blue areas delineate the envelope $[\langle c \rangle \pm \sigma_c]$ of
1035 50 inverse solutions.

1036 **Fig. 7.** Average log hydraulic conductivity $\langle \log(K) \rangle$ (left), standard deviation of $\log(K)$
1037 (middle), and mean error in $\log(K)$ compared to reference (right), for 50 inverse solutions of
1038 test case C1. The reference $\log(K)$ field is at the top of the figure. S1, S2, and S3 correspond
1039 to the three inversion strategies employed.

1040 **Fig. 8.** Average log hydraulic conductivity $\langle \log(K) \rangle$ (left), standard deviation of $\log(K)$
1041 (middle), and mean error in $\log(K)$ compared to reference (right), for 50 inverse solutions of

1042 test case C2. The reference $\log(K)$ field is at the top of the figure. S1, S2, and S3 correspond
1043 to the three inversion strategies employed.

1044 **Fig. 9.** Average log hydraulic conductivity $\langle \log(K) \rangle$ (left), standard deviation of $\log(K)$
1045 (middle), and mean error in $\log(K)$ compared to reference (right), for 50 inverse solutions of
1046 test case C3. The reference $\log(K)$ field is at the top of the figure. S1, S2, and S3 correspond
1047 to the three inversion strategies employed.

1048 **Fig. 10.** Variogram of the reference log hydraulic conductivity (black lines) compared with the
1049 variogram envelopes $[\langle \gamma \rangle \pm \sigma_\gamma]$ (grey areas) calculated over 50 inverse solutions. C1, C2, and
1050 C3 denote the three flow-transport test cases; S1, S2, and S3 correspond to the inversion
1051 strategies.

1052 **Fig. 11.** Reference (left) and simulated (right) solute plumes after 280 days for flow and
1053 transport test case C4.

1054 **Fig. 12.** Solute concentration breakthrough curves at the three locations P11, P7, and P9 (ranked
1055 with increasing distance from solute source) for test case C4. Black lines denote the references;
1056 blue areas delineate the envelope $[\langle c \rangle \pm \sigma_c]$ of 50 inverse solutions.

1057 **Fig. 13.** Average parameters – log hydraulic conductivity $\log(K)$ and porosity ω – (left),
1058 standard deviation of parameters (middle), and mean error in parameters compared to reference
1059 (right) for 50 inverse solutions of test case C4.

1060 **Fig. 14.** Variograms of the reference (black lines) log hydraulic conductivity (left) and porosity
1061 (right) compared with the variogram envelopes $[\langle \gamma \rangle \pm \sigma_\gamma]$ (grey areas) calculated over 50
1062 inverse solutions of test case C4.

1063 **Table 1.** 17 reference studies dealing with coupled flow-transport inversions. Main
1064 characteristics of these studies.

1065 **Table 2.** Main characteristics of synthetic tests cases C1 to C4 inverting coupled flow and
1066 transport to retrieve hydraulic conductivities (and porosity, only test C4).

1067

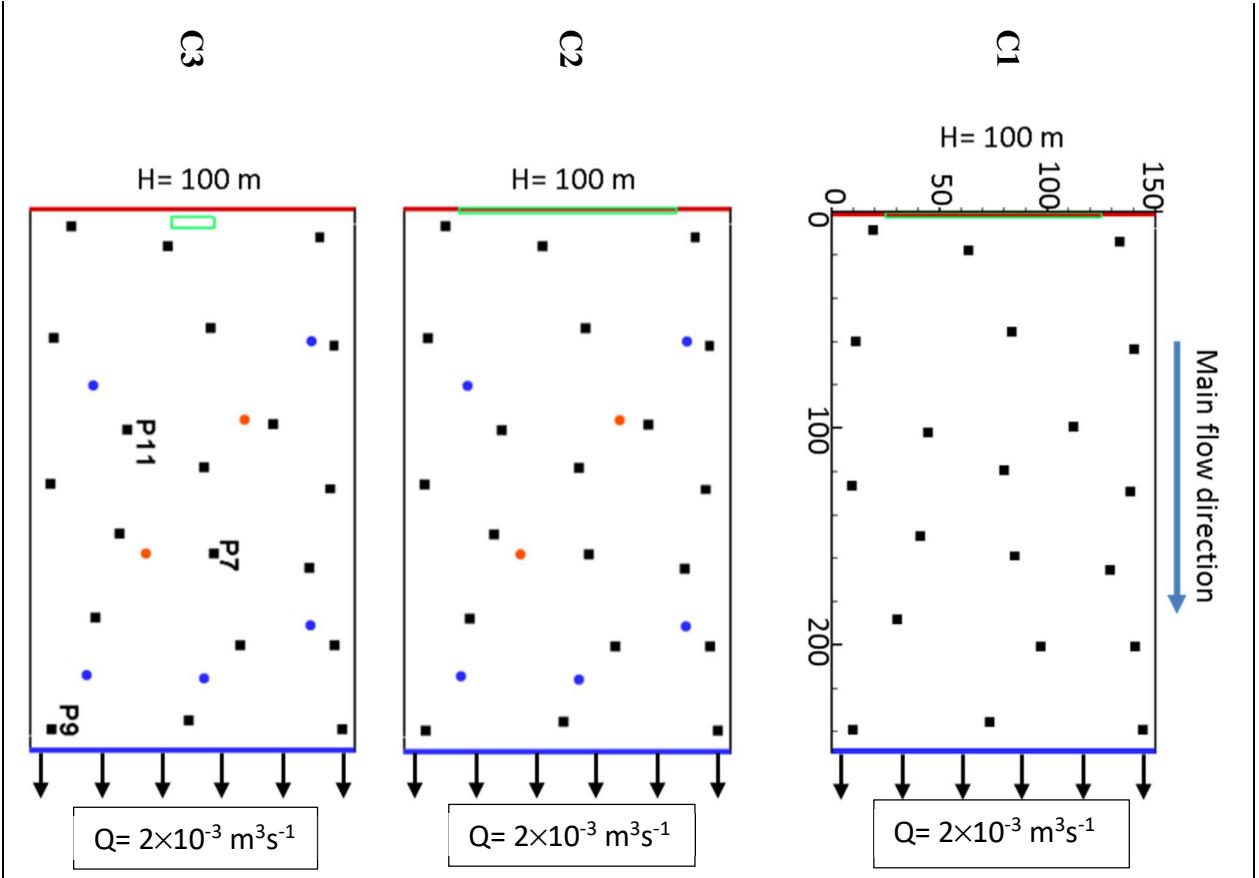


Fig. 1.

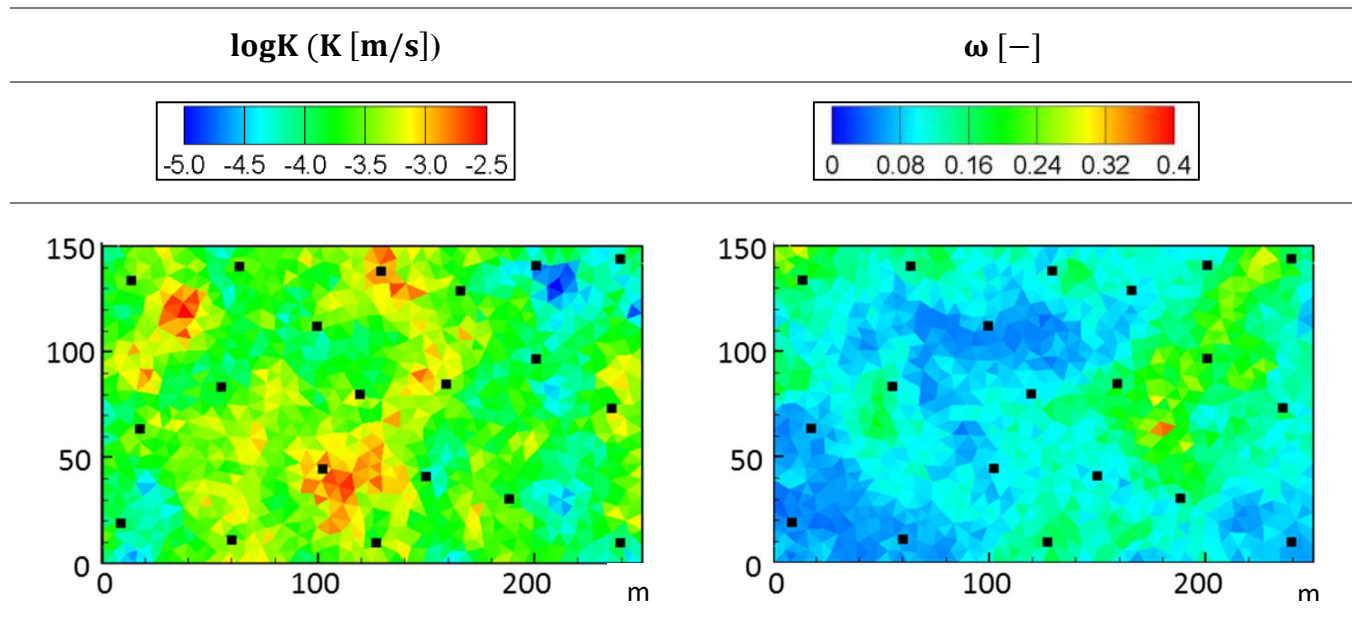


Fig. 2.

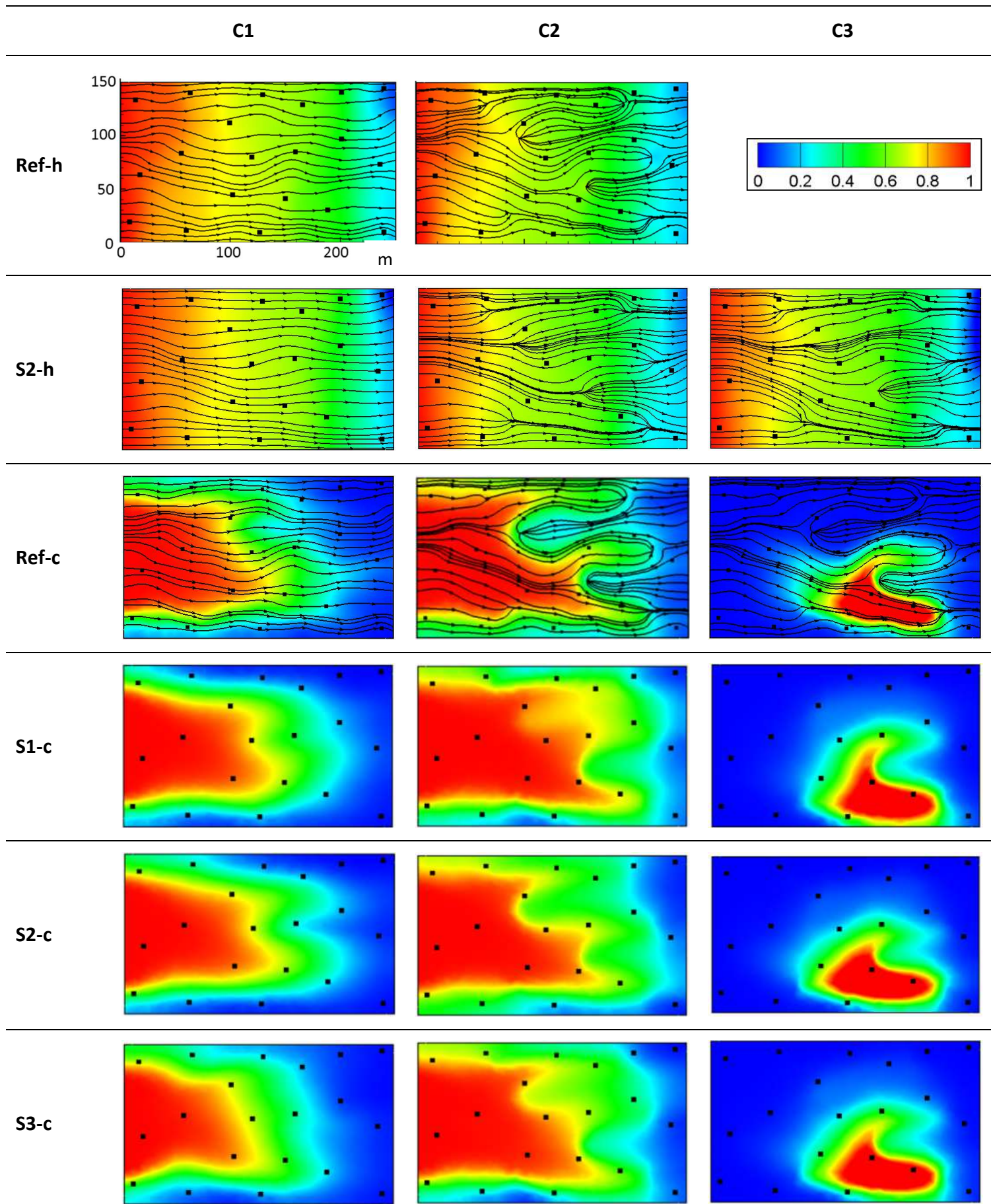


Fig. 3.

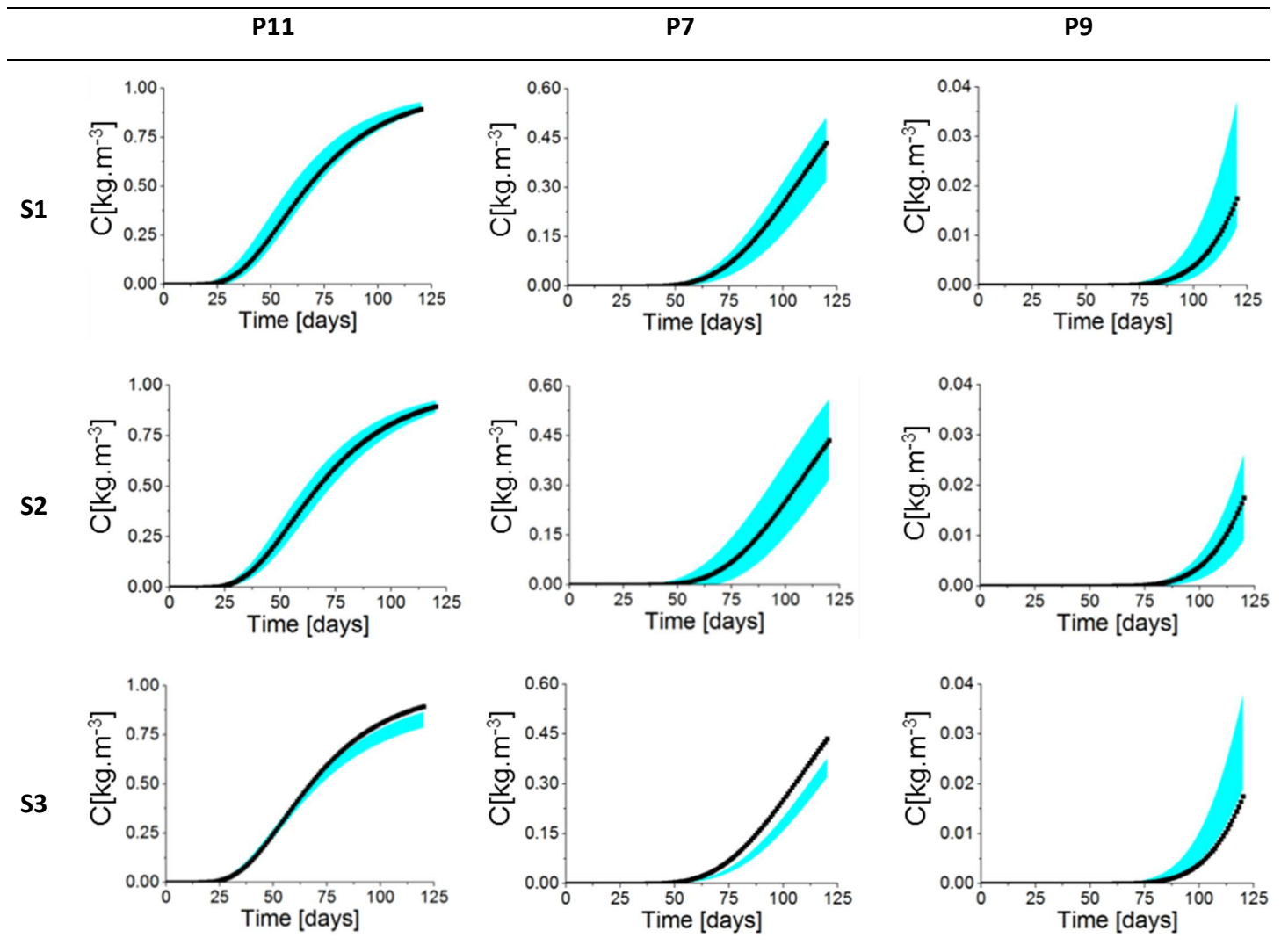


Fig. 4.

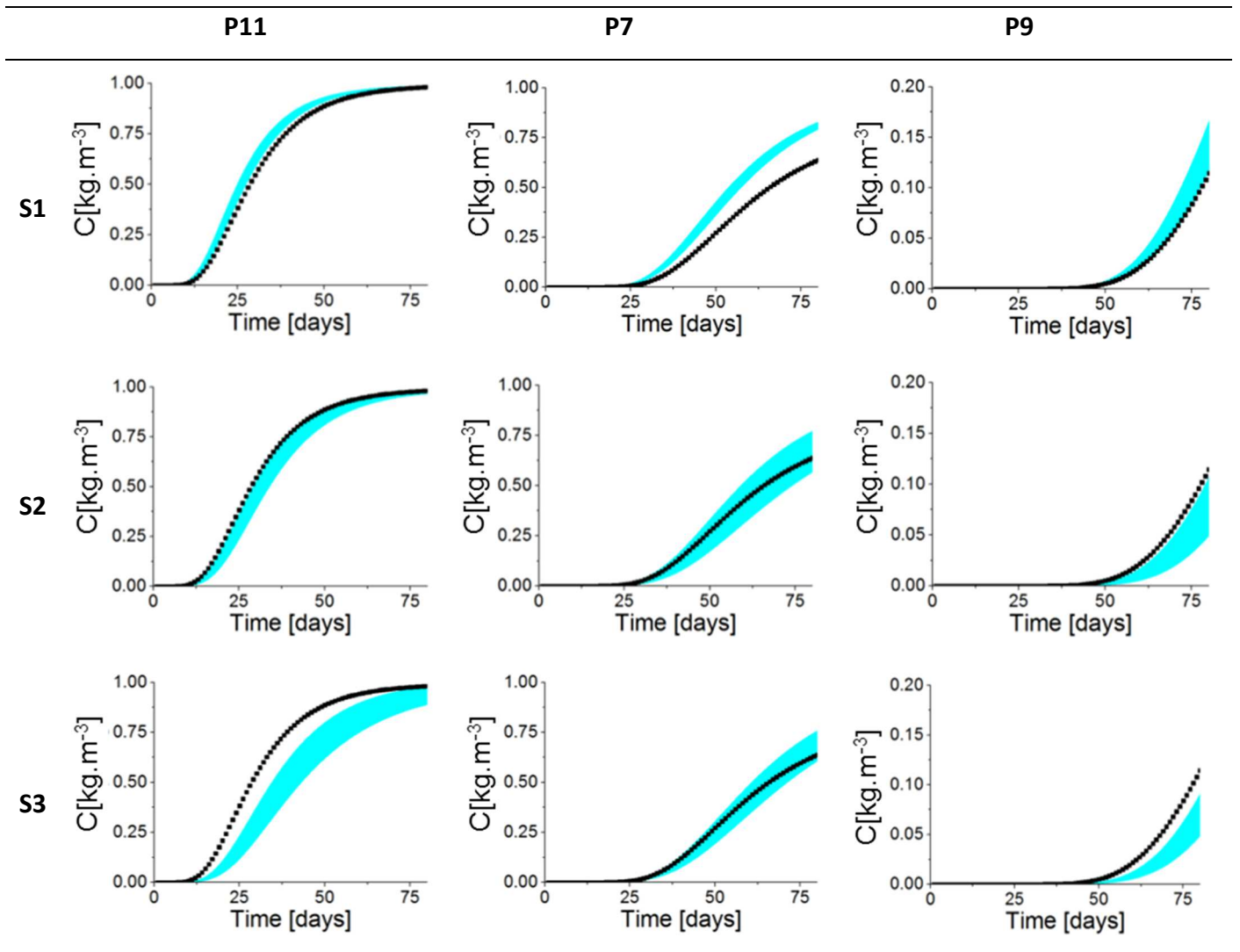


Fig. 5.

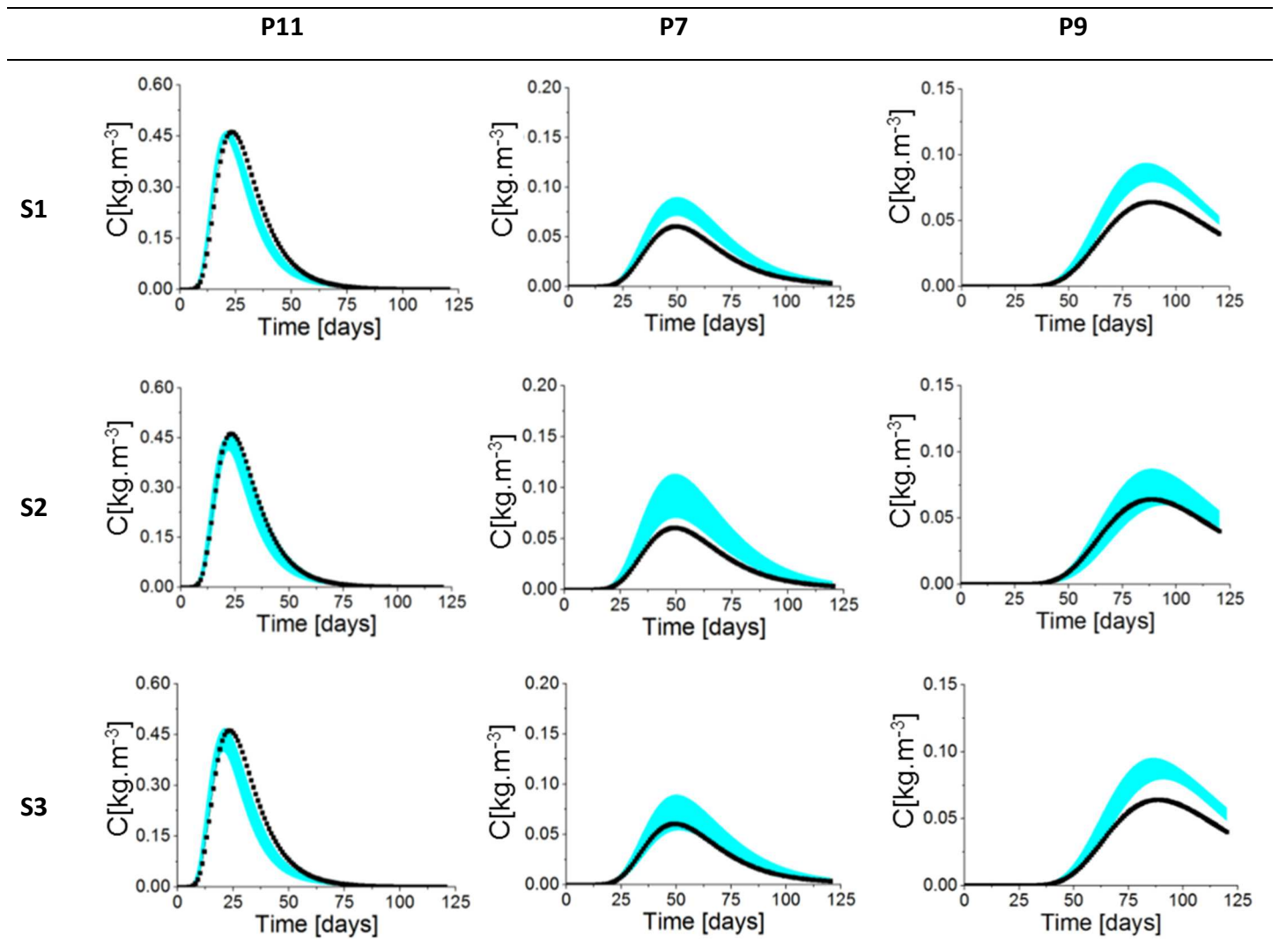


Fig. 6.

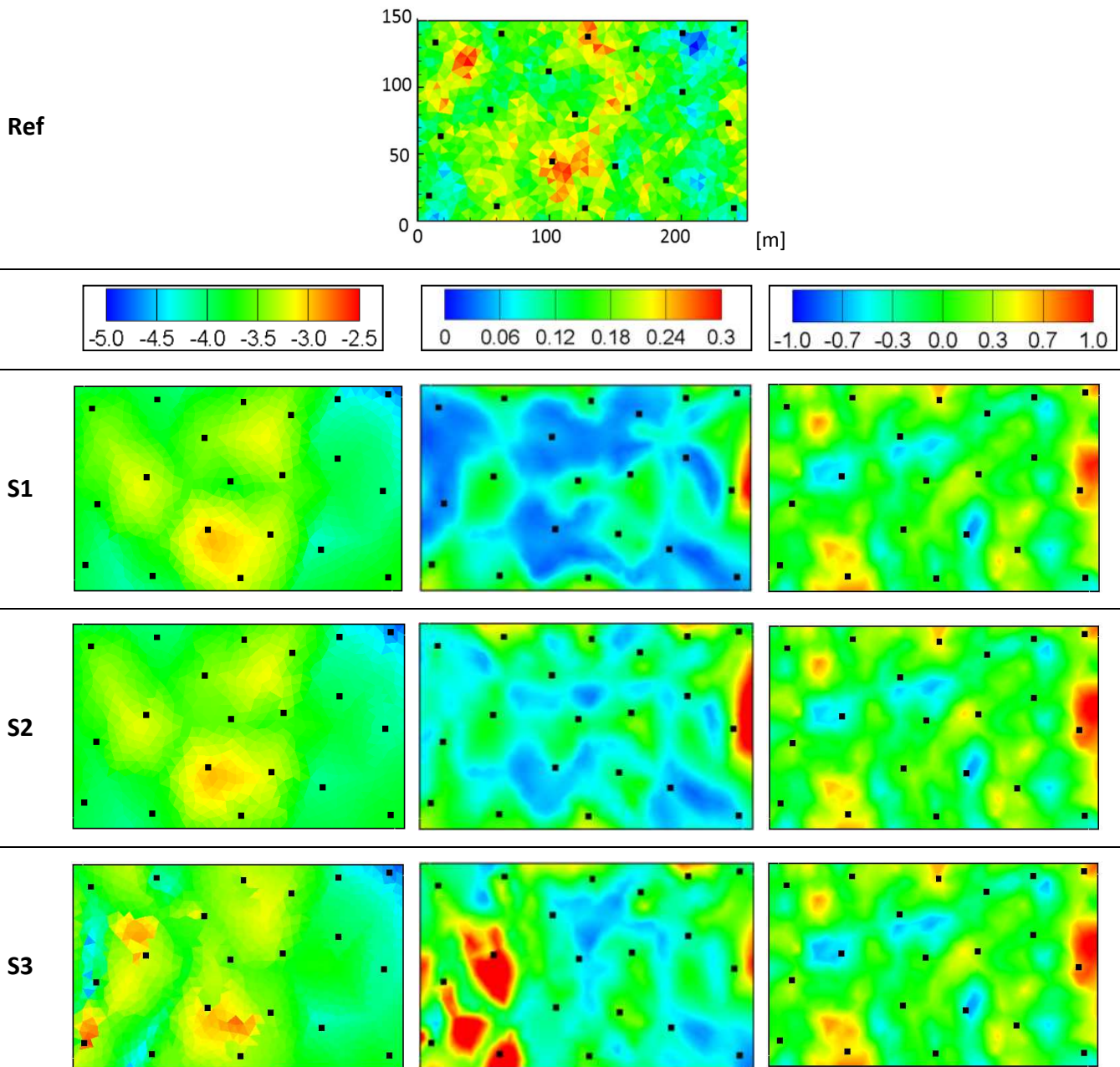


Fig. 7.

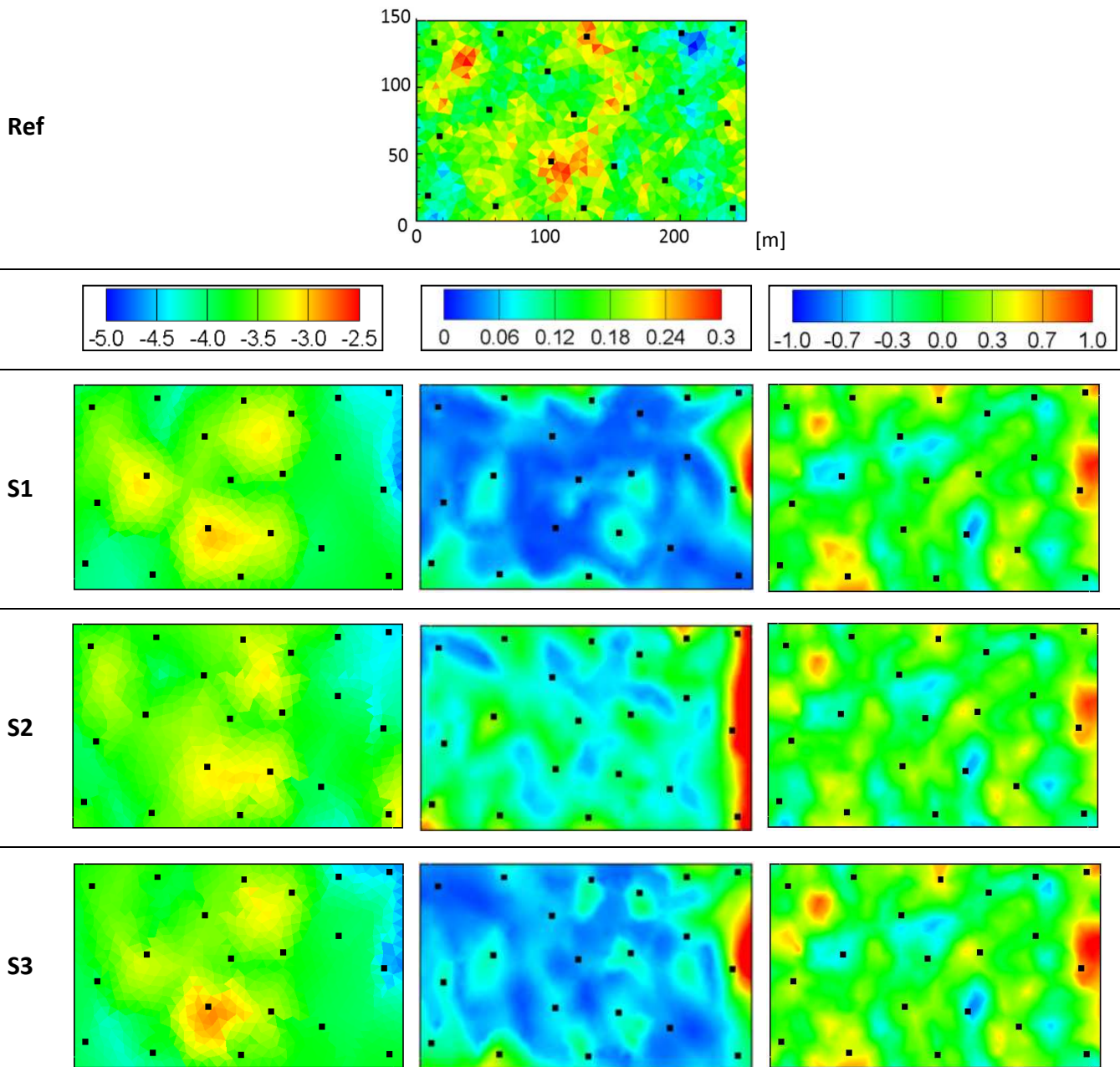


Fig. 8.

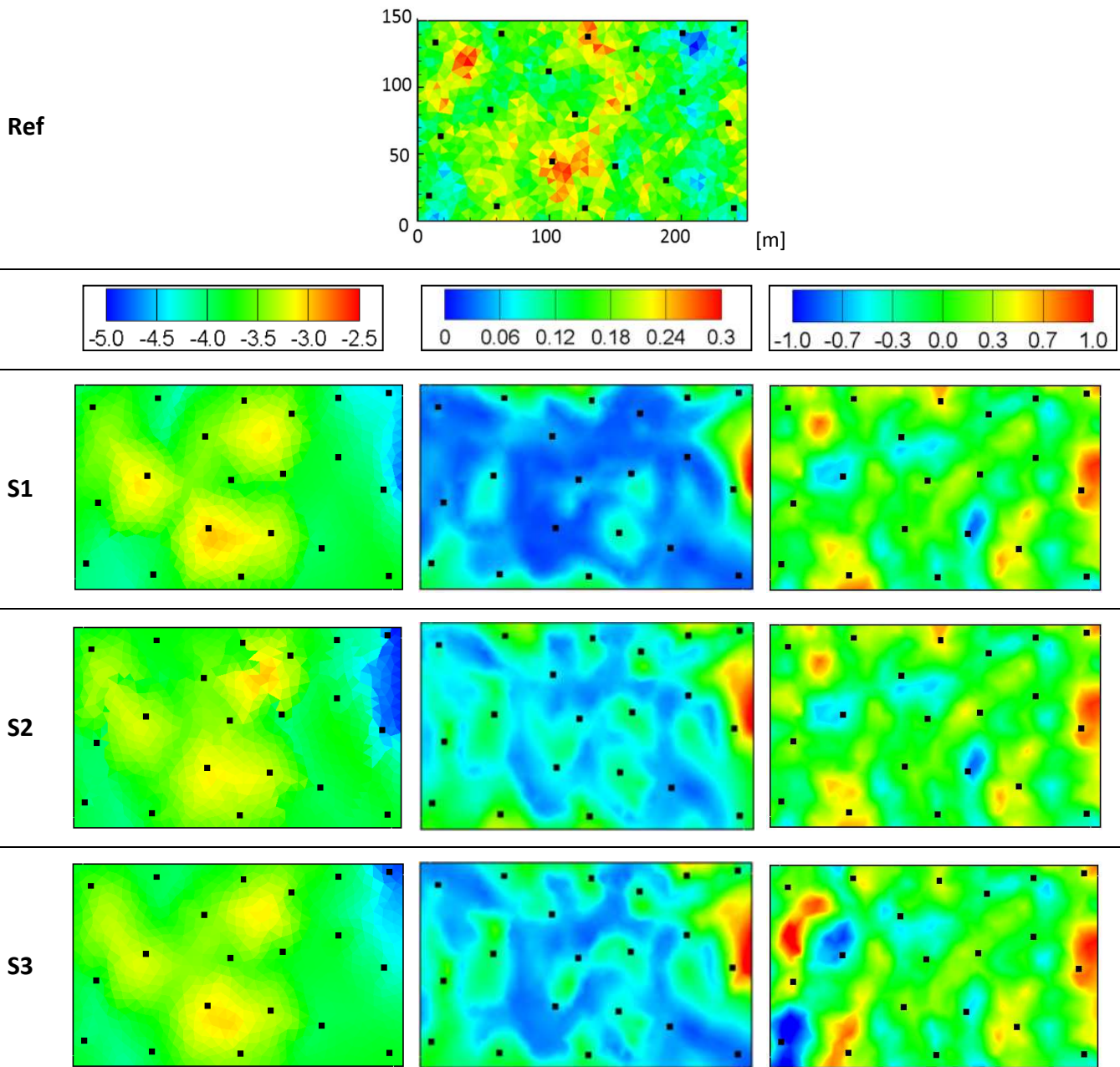


Fig. 9.

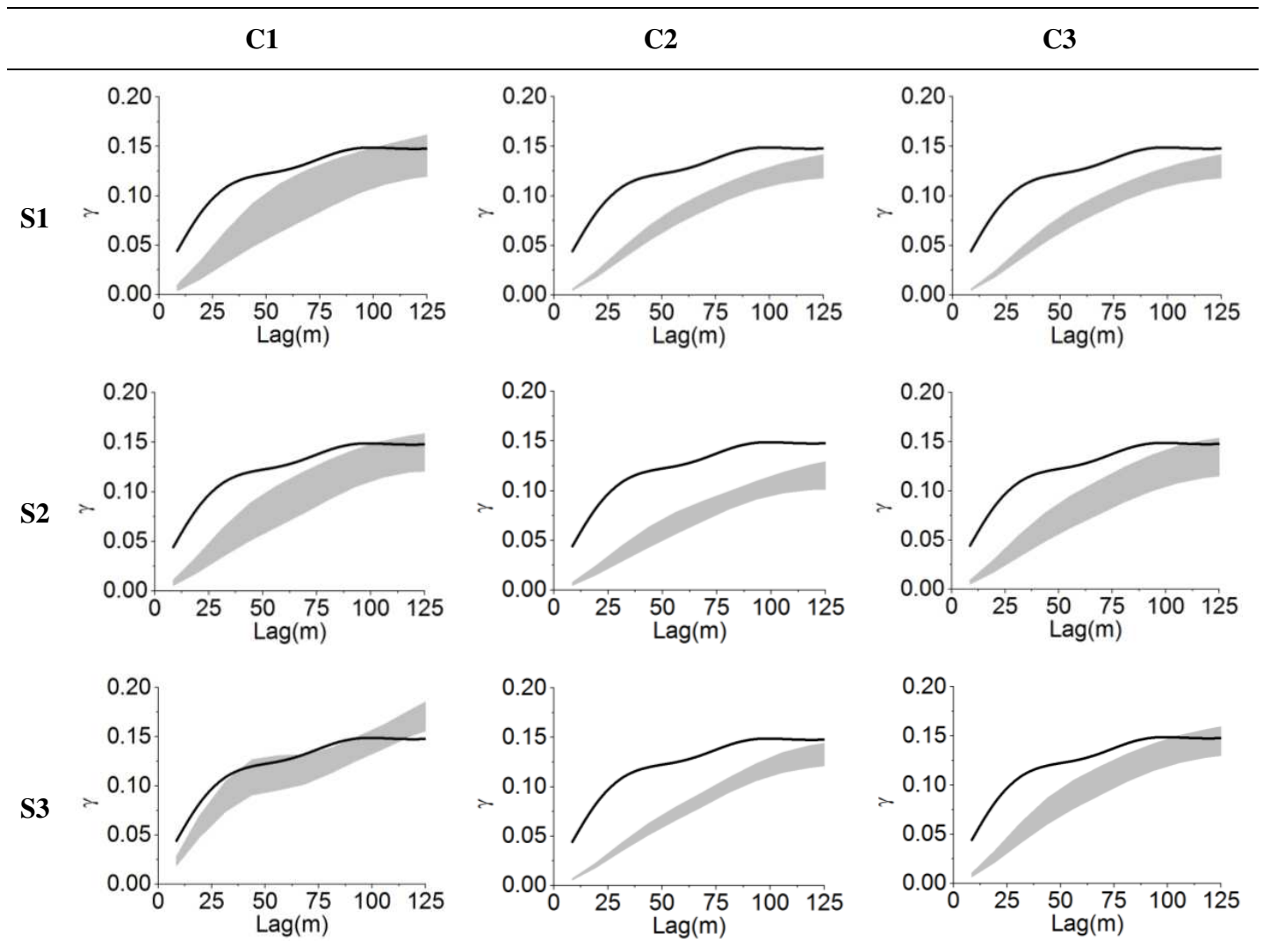


Fig. 10.

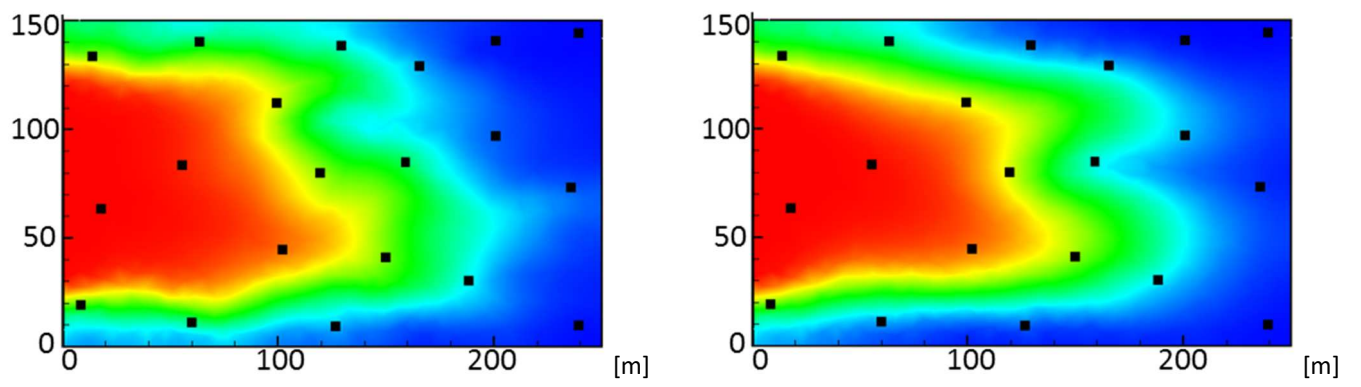
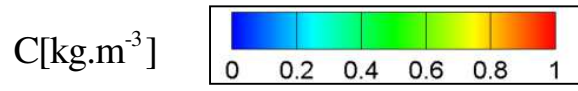


Fig. 11.

P11

P7

P9

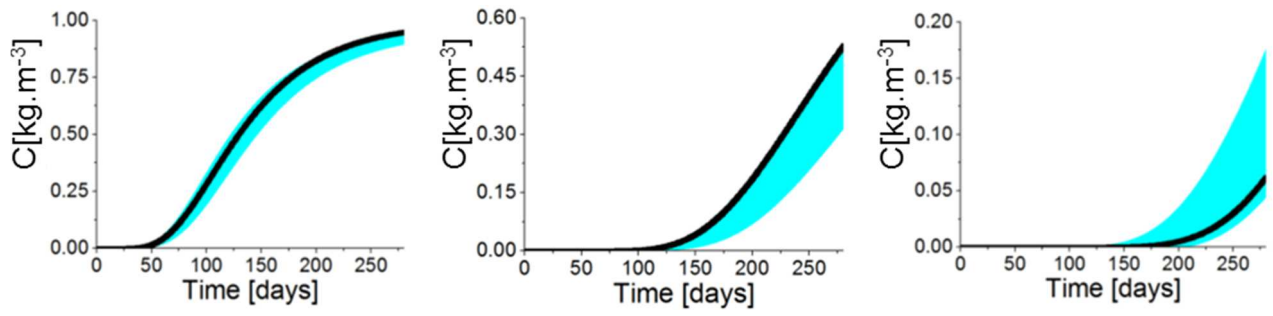


Fig. 12.

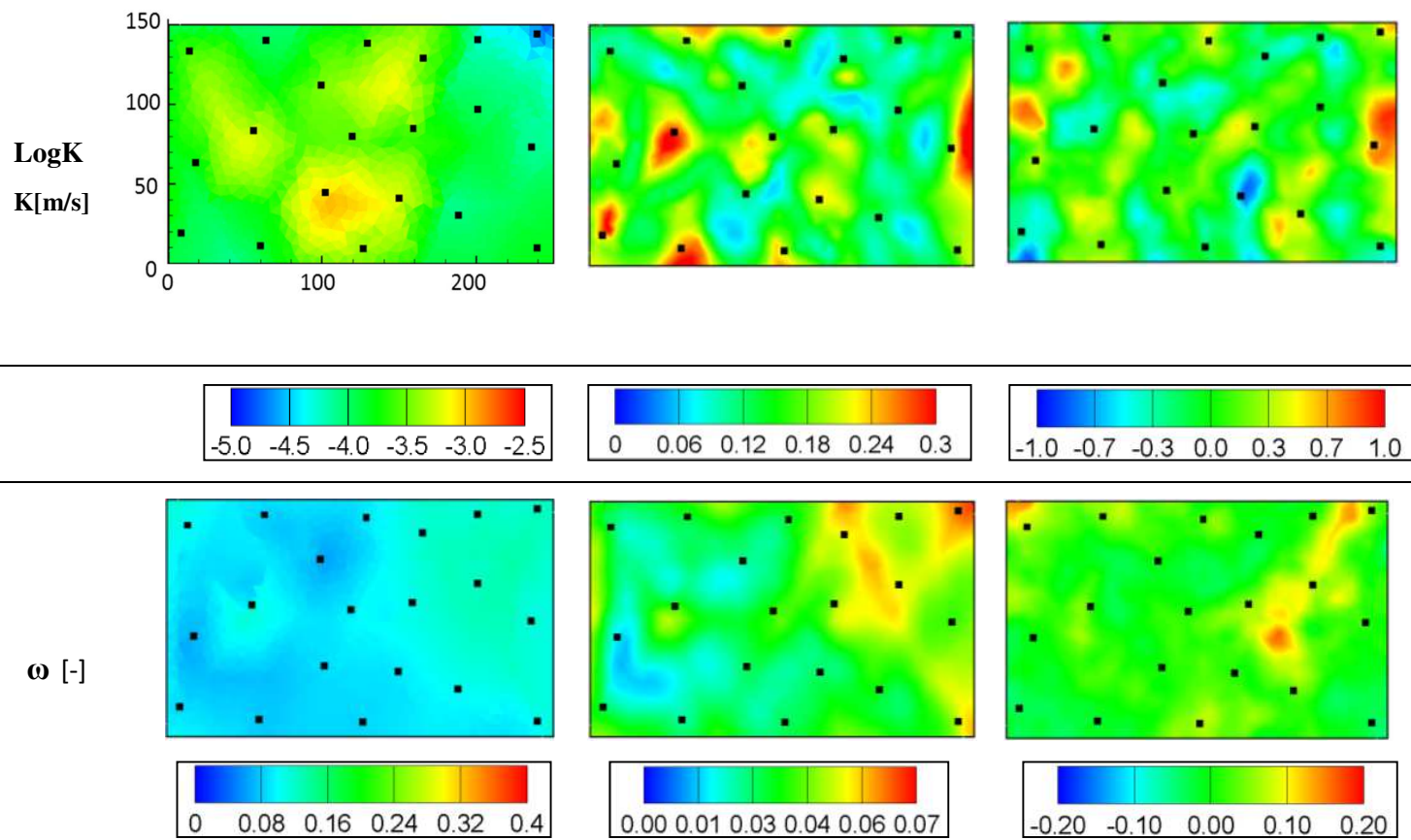


Fig. 13.

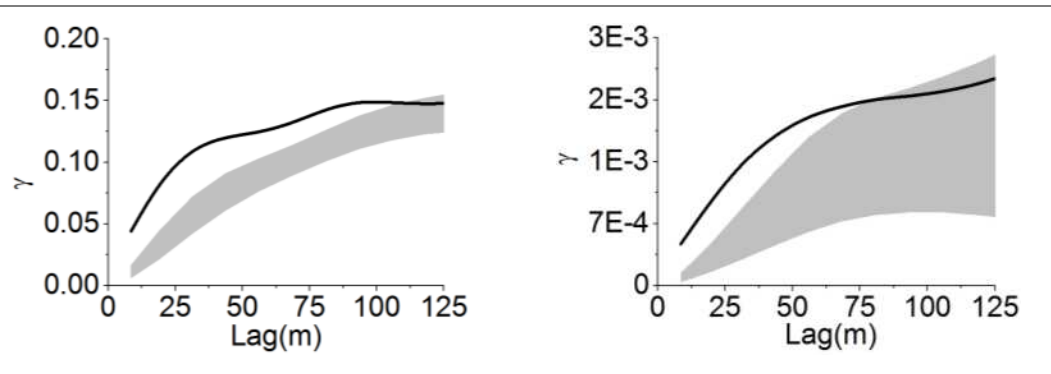


Fig. 14.

Reference	Measured variables	Strategy	Optimization	Parameterization	Estimated parameters
Umari et al., 1979	Transient transport	-	Quasi-linear minimization	Uniform	α Hypothetical test case
Strecker and Chu, 1986	Transient flow and transient transport	Two stage	Gradient-based minimization	Zonation	T, α . Hypothetical test case
Wagner and Gorelick, 1987	Steady flow, transient transport	Simultaneous inversion	Gradient based with adjoint state.	Homogeneous aquifer	K, ω , α . Hypothetical test case
Sun and Yeh, 1990	Transient flow and transport	Simultaneous inversion	Gradient based with adjoint state.	Zonation	K, α . Hypothetical test case
Keidser and Rosbjerg, 1991	Steady flow, transient transport	Two stage with a feedback procedure	Gradient based, Levenberg-Marquardt Gauss Newton	Kriging (pilot points) and/or zonation	Ln(T), α , source concentration. Hypothetical test case
Wagner, 1992	Steady flow, transient transport	Simultaneous with optimized weighting (Carrera, Neuman, 1986a)	Gradient based with adjoint state.	Zonation	K, ω , α , recharge, flux boundary for flow. Source location and mass flux with known hydrogeological parameters. Hypothetical test case.
Hendricks Franssen et al., 2003	Steady state flow, transient transport	Simultaneous inversion	Gradient based with adjoint state.	Stochastic distribution with master blocks	Ln(K), Ln(Ss), Dirichlet for flow, retardation factor, mass sources. Hypothetical test case.
Medina and Carrera, 1996	Steady state and transient flow, transient transport	Simultaneous inversion	Gradient based, Levenberg-Marquardt Gauss Newton	Zonation	Ln(T), α , retardation factor, matrix diffusion, contaminant source strength. Laboratory test case and field case.
Wen et al., 2002	Transient flow and transient transport	Simultaneous inversion	Gradient-based minimization	Stochastic distribution (Sequential self-calibration method)	Ln(K). Hypothetical test case.

Medina and Carrera, 2003	Steady state or transient flow, transient transport	Simultaneous inversion	Gradient based (revised adjoint state), Levenberg-Marquardt Gauss Newton	Stochastic distribution	Ln(T). Hypothetical test case.
Liu et al., 2008	Steady state flow, transient transport.	Simultaneous inversion	EnKF	Stochastic distribution for K, uniform value for other parameters	Ln(K), α , mass transfer rate and mobile porosity ratio. Made experimental site.
Li et al., 2012	Transient flow and transient transport	Simultaneous inversion	EnKF	Stochastic distribution for K and ω	Ln(K), ω . Hypothetical test case.
Pollock and Cirpka, 2012	Steady state flow, transient transport (through temporal moments)	Simultaneous inversion	Gradient-based Gauss-Newton	Stochastic distribution Quasi-linear geostatistical method	Ln(K) and structural parameters by a two steps iterative method. Laboratory experiment.
Kitanidis and Lee, 2014	Steady state flow, transient transport	Simultaneous inversion	Gradient based with Principal Component Geostatistical Approach	Stochastic distribution	Hypothetical test case.
Pool et al., 2015	Transient flow and transient transport	Simultaneous inversion	Gradient based with adjoint state.	Stochastic distribution (regularized pilot points) and geology-based zonation	Ln(T). Field case.
Erdal and Cirpka, 2017	Transient flow, transient transport	Simultaneous inversion	EnKF, Kalman Ensemble Generator	Stochastic distribution for Ln(K) and ω , zonation for recharge.	Ln(K), ω , transient recharge. Hypothetical test case.
Carniato et al., 2015	Transient flow and concentrations of different species. Local values of K, Ss. Lab. scale values for chemical parameters	Three steps: 1. Flow 2. Transport 3. Flow and transport with optimal weighting from Doherty (2003)	Gradient based method. Levenberg Marquardt	Pilot point for K, Ss, recharge.	K, Ss, ω , α , recharge, , degradation rates, mass transfer coefficients. Field site.

EnKF: Ensemble Kalman filter. K: Hydraulic conductivity, Ss: specific storage capacity, T: transmissivity, ω : porosity, α : dispersivity

2
3
4
5

Table 1

	Sink/source for flow	Boundary Conditions for transport	Porosity
C1	No sink/source	Continuous prescribed concentration at the upstream boundary	Known
C2	5 pumping wells and 2 injection wells	Continuous prescribed concentration at the upstream boundary	Known
C3	5 pumping wells and 2 injection wells	Pulse injection	Known
C4	5 pumping wells and 2 injection wells	Continuous prescribed concentration at the upstream boundary	Unknown

Table 2